INVESTIGATING THE PRE-MORTEM DIAGNOSTIC POTENTIAL OF NEUROFILAMENT LIGHT CHAIN IN BOVINE SPONGIFORM ENCEPHALOPATHY

LENA DABBAS

Bachelor of Science, University of Lethbridge, 2023

A thesis submitted

in partial fulfilment of the requirements for the degree of

Master of Science

in

Biological Sciences

Department of Biological Sciences
University of Lethbridge
LETHBRIDGE, ALBERTA, CANADA

INVESTIGATING THE PRE-MORTEM DIAGNOSTIC POTENTIAL OF NEUROFILAMENT LIGHT CHAIN IN BOVINE SPONGIFORM ENCEPHALOPATHY

Lena Dabbas

Date of Defence: March 17, 2026

Dr. Igor Kovalchuk Thesis Co-Supervisors	Professor	Ph.D.
Dr. Waqas Tahir Thesis Co-Supervisors	Adjunct Professor, Research Scientist	Ph.D.
Dr. Nariman Shahhosseini Thesis Examination Committee Member	Research Scientist	Ph.D.
Dr. Andrew Iwaniuk Thesis Examination Committee Member	Associate Professor	Ph.D.
Dr. Dmytro Yevtushenko Chair, Thesis Examination Committee	Associate Professor	Ph.D.

DEDICATION

This thesis is dedicated to my family, who have always been my greatest source of support. To my parents (mom, Ghada, and dad, Mohammad Abd Al Razak Dabbas), who came to a new country and faced every challenge without knowing the language, yet never stopped believing in me, and to my siblings (Douhouk, Rateb, Omar, Safa and Adam) whose encouragement and gentle pushes reminded me to keep going even when things felt difficult. Also, a special thanks to my aunt (Safaa Dabbas), who has been part of the family and whose contribution made a significant impact.

ABSTRACT

Transmissible spongiform encephalopathy is a group of neurodegenerative diseases that affect the central nervous system. They result from the misfolding of a normal cellular prion protein (PrP^{C}) into its abnormal isoform called scrapie prion protein (PrP^{Sc}). These groups of diseases affect different species, including chronic wasting disease (CWD) in cervids, scrapie in sheep and goats, Creutzfeldt-Jakob disease (CJD) in humans, and bovine spongiform encephalopathy (BSE) in cattle. BSE is particularly concerning because it is zoonotic and may cause variant CJD in humans when BSE-contaminated meat is consumed. Diagnosing BSE involves post-mortem testing that requires euthanasia and brain extraction, which is invasive, time-consuming, and expensive.

Given these limitations, it is paramount to explore the potential for BSE detection in live cattle, with surrogate biomarkers being the most promising approach. A candidate biomarker that should be easily detectable in live subjects using a less invasive method, such as blood sampling. In this context, neurofilament light (NfL), a protein biomarker, is well documented in the literature and has been successfully identified in both the cerebrospinal fluid (CSF) and blood in cases of scrapie and CJD.

Since neuronal loss is a key hallmark of prion diseases, and NfL is a marker of neuronal damage, it can be a favourable candidate biomarker. This study examined the potential of NfL as a premortem diagnostic tool for detecting BSE. This was accomplished by assessing NfL regulation in relation to PrP^{Sc} deposition in the brains, followed by analysis of NfL levels in the CSF and blood of both BSE-positive and BSE-negative cattle. Overall, this study is the first to provide evidence of NfL's potential to differentiate between BSE-positive and healthy cattle premortem.

ETHICAL STATEMENT

This research was conducted using banked samples that had been collected previously under appropriate ethical approval prior to the commencement of this study.

ACKNOWLEDGEMENT

I want to acknowledge that without the assistance, guidance, and oversight of my co-supervisor, Dr. Waqas Tahir, the project would not have been completed successfully. I value his leadership in overcoming the project's numerous challenges, his insightful observations throughout the past two years, and his helpful counsel and discussions. I also want to thank my lab members for their training, questions, and critiques, which have enhanced my critical thinking and helped me refine several skills. I am also grateful to Dr. Igor Kovalchuk, my co-supervisor, for allowing me to present my research, share my knowledge, and get constructive feedback. Also, joining his lab helped me engage with other students and seek out different viewpoints, which helped me overcome certain obstacles. I want to thank him for helping me with all the formal documentation required to complete my degree.

Lastly, I would like to express my gratitude to my committee members, Dr. Andrew Iwaniuk and Dr. Nariman Shahhosseini, for agreeing to participate in my master's program, for supporting me throughout my evaluation, for asking valuable questions, and for providing comments on the writing, experimental methods, and statistics. I also want to express my gratitude to the BSE Reference Lab in Lethbridge and the Canadian Food Inspection Agency for allowing me to work with their professionals and experts, and for teaching me how to handle prion material in a high-containment setting. I am grateful to the BSE reference lab for providing me with all the supplies I needed to carry out my research project, including animals infected with BSE.

Table of Content

LIST OF TABLES

LIST OF FIGURES

LIST OF ABBREVIATIONS

BH	Brain Homogenate
BSE	Bovine Spongiform Encephalopathy
CJD	Creutzfeldt-Jacob Disease
CNS	Central Nervous System
CSF	Cerebrospinal Fluid
CWD	Chronic Wasting Disease
NfL	Neurofilament Light Chain
PrP^{C}	Cellular Prion Protein
PrP^{res}	Prion protein resistant core
PrP^{Sc}	Scrapie Prion Protein
TSE	Transmissible Spongiform Encephalopathy
SEM	Standard Error of Mean
SRM	Specific Risk Material

1. Introduction

1.1. Prion Diseases

These are a group of neurodegenerative diseases, alternatively known as Transmissible Spongiform Encephalopathies (TSEs), caused by a pathogenic agent known as prion [1]. Such a group of diseases is striking, as neither bacteria nor viruses cause them. Instead, prions are protein particles formed by the misfolding of normal cellular prion protein (PrP^{C}) into a pathogenic form (PrP^{Sc}). Once misfolded, these proteins become infectious by forming large aggregates in the central nervous system (CNS), leading to neuronal damage, neuronal dysfunction, and eventual cell death, leading to degeneration of the brain [2]. These diseases manifest in a variety of species, including humans and animals, such as Creutzfeldt-Jakob disease (CJD) in humans [3], chronic wasting disease (CWD) in cervids. [4], scrapie in sheep and goats [5], and bovine spongiform encephalopathy (BSE) in cattle [6].

1.1.1. Properties of PrP^{C} and PrP^{Sc}

These proteins have a central core that resists degradation [6, 7], Although the molecular basis of how PrP^{C} transforms into PrP^{Sc} remains unclear, prions lack nucleic acids and replicate by recruiting host-encoded PrP^{C} [6]. The conversion of PrP^{C} into abnormal PrP^{Sc} involves conformational changes that significantly alter PrP^{C}'s functions and features, rendering it highly infectious properties. In their physiological form, PrP^{C} are mainly composed of alpha helices, accounting for 43% of the entire structure. In contrast, in their misfolded form, PrP^{Sc}, most alpha helices are converted into beta sheets, which make up 42% of the overall structure, compared to 3% in the physiological configuration

[1, 5, 7]. Those beta sheets are necessary for providing the stability needed by PrP^{Sc}, thus facilitating oligomerization and elongation of fibrils and leading to the formation of larger aggregates that are difficult to break down [6], thereby damaging neurons by interfering with neuronal cell function [5, 8].

The physiological form of these proteins, PrP^{C}, are considered essential for the cell due to their roles in cellular processes. They are involved in neuronal development, as evidenced by PrP^{C} knockout mouse models showing reduced neuronal precursor cell proliferation [27], and in cell adhesion, differentiation, and cell-to-cell communication [28, 29]. Interactions of PrP^{C} with other proteins are important for extending neurites, guiding axons, and promoting synapse formation [29], neuroprotection [30, 31]. Additionally, they participate in the production and maintenance of myelin [21, 22], control ion uptake and detoxify excess ions in the nervous system [32, 33], and take part in signal transduction [34, 35] and the regulation of circadian rhythms [36]. Therefore, the proper three-dimensional structure of these proteins is essential for them to perform their functions effectively [37].

Structural changes in prion proteins because of misfolding, can lead to a loss of their physiological functions and the acquisition of toxic effects. The creation of PrP^{Sc} and its accumulation in cells impair the neuroprotective role of PrP^{C} by interfering with autophagy and lysosomal systems that break down aggregated proteins [9-11]. Additionally, trafficking of PrP from the ER is disrupted, leading to reduced translation, weaker neurons, synaptic loss, and cell death [12-15]. Moreover, misfolding can trigger toxic pathway cascades similar to those observed in Alzheimer's disease, including kinases, that disrupt cellular functions [16-20].

1.2. Bovine Spongiform Encephalopathy

The BSE is a prion disease of cattle, which causes PrP^{Sc} deposition and aggregation primarily in the CNS, leading to progressive neuronal damage and spongiosis in the brain [21, 22]. The first case of BSE was found in the UK in 1986, and it soon developed into an epidemic [20, 21]. Later, BSE in cattle was linked to a prion disease in humans, variant CJD, which was believed to be caused by the consumption of BSE-contaminated meat, indicating that BSE was a zoonotic disease [23, 24]. In the meantime, BSE had spread globally through trade and the exchange of infected cattle, allowing the disease to reach various other countries, including Canada. Canada reported its first case of BSE in 1993, and after confirmation, it was determined that the cattle had been imported from the UK. Later in 2003, the first Canadian-born case was identified, leading to subsequent huge economic losses from the ban on international trade of Canadian cattle and their products and heightened public health concerns over potential transmission to humans [25]. In response to the rise of this epidemic, the Canadian government implemented strict new measures to control the spread of the disease, including the establishment and enforcement of an enhanced surveillance program for BSE and a ban on the inclusion of specified risk materials (SRM) in human food and animal feed [26, 27]. The SRM refers to tissues from affected cattle in which prions are highly prevalent, which include the skull, brain, trigeminal ganglia, eyes, tonsils, spinal cord, and dorsal root ganglia for calves 30 months of age or older and the distal ileum for calves of all ages [6, 22, 28]. The program aimed to control the risk of BSE transmission to human and cattle by eliminating the recycling of the pathological agent (PrP^{Sc}), and indeed, it proved successful in reducing the overall number of BSE cases in Canada. The success of this program helped Canada gain

recognition from the World Organization for Animal Health (WOAH) as having negligible BSE risk in 2021 [29]. This model facilitated collaboration between the Canadian government and the cattle industry to mitigate the risk of BSE [25]. As part of these mandates, all farmers and animal facilities were required to comply with those measures by keeping detailed records of animal identification and tracking any potential clinical signs of BSE. These signs include but not limited to, low head carriage, ataxia, incoordination, inability to rise, losing weight, low milk production, aggressive behaviour, sensitivity to light, teeth grinding, and hesitation against any obstacles [6, 22, 30, 31]. Thus, when these symptoms are combined with age, it is what makes an animal a BSE candidate [6, 22, 30, 31].

At any point, if an animal becomes a BSE candidate based on the presentation of relevant clinical signs and qualifying age, they must be euthanized, and brainstem must be extracted and tested using a validated rapid surveillance screening test (e.g., Bio-Rad TeSeE ELISA) to identify the presence or absence of the pathogenic agent, PrP^{Sc} [32, 33]. Following initial screening, if the results are initially reactive, a confirmatory test using immunohistochemistry or Scrapie-associated fibrils (SAF) immunoblot must be performed on the brainstem at the level of obex [34, 35]. However, there is currently no valid ante-mortem test available for screening live animals, and the only option for screening for BSE is limited to autopsy. Thus, preventing early disease detection because the pathological agent is primarily located in the CNS [36, 37], which underscores the need to investigate and develop potential diagnostic tools to detect BSE in live animals.

What further complicates prion diseases is their long incubation periods (up to decades) [38], which delays symptom onset; thus, animals can remain silent carriers for many years before exhibiting clinical symptoms. Once clinical signs become

visible, it means that the disease has progressed substantially, and the animals would die shortly after, as the pathogenic agent would have manifested in its advanced stages, causing irreversible damage [21, 39-42].

Having more than one type makes BSE more concerning and adds another layer of complexity to the disease. BSE has two forms: classical (C) BSE, which results from ingesting feed contaminated with BSE [29, 30], and atypical, which develops spontaneously [31] in older cattle. Atypical BSE also has two subtypes, classified as low (L) or high (H), which differ in their biochemical properties, as visualized on a Western blot, including the molecular mass of PrP^{Sc} [29,31].

Considering three strains of BSE, it is important to identify the type in case of a BSE positive animal, as each strain may reflect distinct routes of spread and therefore different associated risks. For example, from the perspective of disease control measures, identifying C-BSE, would mean contamination of animal feed with a TSE agent, require back tracing to track the point of contact of animal feed with a TSE agent to eliminate the source of contamination. Due to the fact that C-BSE in cattle occurs due to the consumption of a contaminated feed would also mean possibly more animals being exposed to the same contaminated feed, potentially more cases, hence requiring culling and more testing and lastly resulting in international trade restrictions on livestock and livestock products. However, this can be different if there is an H type or L type BSE case, as atypical BSE is spontaneous in nature and has less impact on international trade. However, back tracking to ensure the carcass of an affected animal, irrespective of the type of BSE, is secured appropriately to prevent its entry into food or feed chain will be still required.

For distinguishing the three types of BSE, western blot is a vital tool as it assesses the molecular weights of the prion proteins' resistant core. Prion protein shows three distinct

bands in western blot due to saccharide occupancy at the two N-glycan sites, Asn181 and Asn197, resulting in three possible forms of PrP such as diglycosylated, mono-glycosylated, and non-glycosylated. However, the percentage compositions of each glycoform (di, mono, un) vary between BSE strains forming a glycoform profile, and the relative sizes of those bands also differ [43, 44]. These biochemical features are quite conserved between these types of BSE and very helpful in accurately distinguishing between various types of BSE through western blot.

1.3. Premortem Detection of BSE

Currently, there is no pre-mortem test available to detect BSE, and developing such a test would be promising, as it could help prevent the accidental introduction of the disease into the food and feed supply. If such an approach is developed, it could enable early detection of clinical suspects and removal from the population. While pre-mortem detection of BSE is limited, testing surrogate biomarkers is well established in many neurodegenerative diseases, including those affecting humans. Biomarkers like Tau and 14-3-3 are known to aid in diagnosing several human neurodegenerative diseases like Alzheimer, dementia, Parkinson, ALS, and CJD [49-51]. A similar strategy has not yet been employed for TSEs in the livestock sector, highlighting the need for further research into early diagnostic methods for animal neurological disorders, such as BSE [52]. However, the above-mentioned biomarkers have limitations, mainly because they are detectable only in cerebrospinal fluid (CSF) and not in blood [53]. While CSF can be collected from humans, obtaining it from animals is invasive and challenging, making it less practical for animal studies.

Recent studies have identified a new, more promising biomarker candidate: neurofilament light chain (NfL). NfL is a cytoskeletal protein that has attracted significant attention in the field of neurodegenerative diseases, as it can be readily detected in both CSF and blood, making it an ideal marker of neuronal damage and a potential pre-mortem diagnostic tool [45]. Numerous studies have demonstrated that measuring CSF NfL levels can aid in the differential diagnosis of CJD and neuronal damage [45, 46]. Moreover, the NfL was successfully captured in a variety of prion diseases, including scrapie in sheep and CJD in humans and was found elevated in both CSF and blood [47]. Given the similarities in the pathogenesis of prion disease in humans and animals, as BSE shares relatively high sequence homology (86%) with humans [11], NfL appears to be a potential biomarker that could provide a realistic pre-mortem diagnostic approach for BSE.

The NfL plays a role in maintaining axonal stability and growth and is mainly expressed in myelinated axons, which support axonal development and function [48, 49], and is a core factor in the cytoarchitecture and function of neurons [50-54]. Following axonal injury or neurodegeneration, NfL is released from damaged neurons into the extracellular space, increasing its concentration in cerebrospinal fluid (CSF) and eventually in blood [47, 50]. This release of NfL can also result from normal aging and maturation processes; therefore, the detected NfL level can serve as an indicator of the degree of brain damage. Thus, the NfL does not merely serve as a biomarker of neuronal damage; it also indicates the severity of damage at any point in time during neuronal-damaging disorders [28].

The NfL serves as a diagnostic marker for neurodegenerative diseases in humans, as it can detect neuronal damage caused by infections and prion-related diseases. While NfL shows strong potential as a biomarker for various prion diseases, we hypothesize that NfL can differentiate between BSE-positive and BSE-negative animals' antemortem. To prove

this, comprehensive validation and further research are required before it can be used for pre-mortem detection of BSE. Improving detection methods to make BSE and prion disease diagnoses more consistent and reliable is essential in enhancing pre-mortem diagnostic capabilities.

1.4. Objectives

This research aims to investigate NfL as a biomarker for neuronal damage in BSE. It can provide a quick, non-invasive way to detect BSE in live animals. To achieve this, the project includes three specific objectives.

I. Examining the link between PrP^{Sc} deposition and NfL spatial regulation in post-mortem brains of cattle challenged intracranially with BSE-positive and negative brain homogenate. Since NfL is a well-known biomarker of neuronal damage, this will help understand how NfL levels associate with PrP^{Sc} deposition across the CNS during the pathogenesis of prion disease in BSE.

II. After examining the spatial regulation of NfL and its association with PrP^{Sc} in the brain, it is crucial to measure its levels in the post-mortem CSF of both BSE-positive and negative cattle. This will help determine whether NfL can distinguish between BSE-negative and positive animals and compare these findings with previous studies on NfL in sheep and humans.

III. Then, the project's milestone will be to assess NfL levels in premortem blood samples from animals that were experimentally challenged, with blood collected while the animals were still alive. This step is crucial to the study as it will evaluate whether NfL provides a less invasive method for differentiating between BSE-positive and negative animals while they are still alive.

Investigating the use of NfL as pre-mortem biomarkers could enable early detection of BSE in living animals. If proven effective, this research might support the development of new methods for diagnosing neurodegenerative diseases in animals, potentially improving animal health globally.

2. Materials and Methods

2.1. Experimental Design

To explore the potential of NfL as a biomarker for neuronal damage in BSE, it was essential to investigate and establish the relevance of NfL regulation during BSE pathogenesis and to determine whether NfL could distinguish between BSE-positive and BSE-negative animals in body fluids such as CSF and blood without requiring euthanasia. First, to assess relevance, NfL and PrP^{Sc} levels were determined in various regions of the CNS using an Enzyme-Linked Immunosorbent Assay (ELISA) for NfL and an IDEXX HerdChek 43-13466-00 antigen-capture enzyme immunoassay (EIA) for $PrP^{Sc,}$ respectively. These results for NfL and PrP^{Sc} were further validated by immunohistochemistry (IHC). For these experiments, a total of 12 animals were used, with n = 3 per group: negative control, C-BSE, H-BSE, and L-BSE, as shown in Table 1. Of these animals, seven CNS regions were included. Outcomes from NfL ELISA, IDEXX-EIA, and IHC experiments were analyzed to assess the correlation between NfL regulation and PrP^{Sc} deposition across multiple brain regions.

Second, to investigate the potential of NfL to differentiate between BSE-positive and BSE-negative animals, NfL levels were analyzed in postmortem CSF samples from BSE animals (n=13; including C-BSE=5, H-BSE=2, L-BSE=2) and compared with those in

healthy control animals (n=4). This was achieved by using the Quanterix NF-Light ELISA kit for CSF (Uman Diagnostics, 10-7002-RUO).

Last, to explore the potential of NfL to differentiate between BSE-positive and BSE animals antemortem, NfL levels were measured in the antemortem serum samples of BSE (n=15; including C-BSE=6, H-BSE=3, L-BSE=3) and healthy control animals (n =3) using the Quanterix NF-light ELISA kit for serum (Uman Diagnostics, 20-8002-RUO). Outcomes of these experiments were further analyzed to determine the specificity and sensitivity of NfL for diagnosing BSE antemortem in clinical serum samples from live animals.

Throughout this project, all examined CSF and serum samples were previously stored for extended periods. Some were used in other studies, exposing them to freeze-thaw cycles and varying storage temperatures, especially during freezer malfunctions. Therefore, to ensure these factors did not influence the results, it was necessary to assess whether exposure to multiple freeze-thaw cycles and different storage temperatures affected NfL levels due to degradation, as described in [58, 59]. Stability assessment was achieved by intentionally exposing CSF and serum samples from C-BSE animals to multiple freeze-thaw cycles and different storage temperatures and comparing them with samples that had not been exposed to these conditions. The evaluation was conducted by testing NfL levels in CSF and serum samples using CSF- and serum-specific NfL ELISA kits, respectively, and evaluating the results to determine the impact of environmental conditions on NfL levels in these samples.

2.2. Materials:

BSE-positive brain materials, along with controls, were obtained from the in-house animal library at the Canadian BSE reference laboratory, National Centre for Animal Disease (NCAD) in Lethbridge. Regions of the CNS analyzed included frontal cortex (FC), thalamus (Th), hippocampus (Hp), occipital cortex (OC), obex (Ob), cerebellum hemisphere (CH), and cerebellar peduncle (CP). All of these tissues belonged to cattle that had been experimentally challenged via intracranial inoculation (i.c.) using brain homogenates (BH) from different types of confirmed BSE cases (C, H, and L) or from healthy cattle. Calves exposed to BH from healthy cattle served as negative controls and were housed together with calves challenged with BSE-positive material. Briefly, upon arrival at the laboratory, the calves were examined, tagged, and housed in the biocontainment level 3 unit. To reduce stress, all animals were kept together and provided with appropriate care, including feed and water. Before inoculation, the animals were closely monitored daily to ensure they remained perfectly healthy.

After one-week of acclimation period, the animals were sedated using a mixture of xylazine and ketamine, as described for those animals in a previous study [55]. For a local anesthetic, a small incision was made to facilitate Lidocaine injection into the midbrain. A 22-gauge needle was used to create a 1.6 mm hole in the skull, into which 1 mL of 10% BH was directly administered into the midbrain at the junction of the parietal and frontal bones. Once the BH inoculation was complete, the skin on the skull was sutured, and antibiotics were administered. For 30 days post-challenge, the calves were kept in biocontainment level 3, after which they were moved outdoors to a bio-confinement.

At that point, all calves were monitored daily by animal care staff and weekly by a veterinarian and project lead to evaluate their clinical health until any signs appeared, mainly determined by the animal's inability to rise, loss of appetite, and loss of body condition. Once clinical signs were observed, the animals were immediately euthanized, and their brain tissues were collected during necropsy in the presence of a pathologist. This enabled accurate identification and separation of various regions of the CNS for subsequent analysis. However, in the control group, the animals' lifespans were predetermined. At post-mortem, all collected brain tissues were divided into two halves: one stored at -80°C for molecular analysis, and the other fixed in formalin for histology and immunohistochemistry. Additionally, post-mortem CSF was collected, aliquoted, and stored at -80°C until further analysis. Blood samples were regularly taken every six months throughout the animals' lifespan, with the last blood samples collected just before euthanasia. The blood samples collected just before euthanasia were referred to as clinical blood samples and were used for ante-mortem analysis at the clinical stage in this study. These blood samples were processed at the time of collection to separate serum and plasma, which were stored at -80°C for future use. Table 1 provides a comprehensive overview of all animals included in this study.

Table 1: Summary of all intracranially (IC) challenged animals used in the study. X denotes that a sample was available, whereas NA denotes that a sample was not available.

Animal ID	Age at Inoculation (months)	Inoculum	Inoculation route	Age at Euthanasia (months)	Brain	CSF	Blood
27022	7	Control	IC	18.8	X	X	NA
27031	7	Control	IC	17.9	X	X	X
27029	7	Control	IC	33.9	X	X	X
29059	5	Control	IC	19.8	Substitute	X	X

25015	7	C-BSE	IC	25.6	X	X	X
25022	7	C-BSE	IC	27	NA	X	X
25023	7	C-BSE	IC	26.9	NA	X	X
25032	7	C-BSE	IC	26.1	NA	X	X
29024	5	C-BSE	IC	19.7	X	X	X
29026	5	C-BSE	IC	18.4	X	X	X
21429	6	H-BSE	IC	74.8	X	X	X
29018	5	H-BSE	IC	17.7	X	X	X
29033	5	H-BSE	IC	17.3	X	X	X
21406	6	H-BSE	IC	79.7	X	X	NA
29012	5	L-BSE	IC	17.9	X	X	X
21419	6	L-BSE	IC	64.2	Substitute	NA	X
29030	5	L-BSE	IC	17	X	X	X

2.3. Methods:

2.3.1. Evaluating PrP^{Sc} Levels in the Brain Using ELISA IDEXX HerdChek

PrP^{Sc} levels in different regions of the CNS of BSE-challenged animals (C-, H-, and L—type BSE; n = 3) and respective controls (n = 3) were determined using a commercial IDEXX—EIA kit on BHs [22, 56]. Briefly, the tissues weighing approximately 0.30 ± 0.05 g were trimmed and homogenized in an IDEXX homogenization buffer. For homogenization, the tissue samples were processed through the Fisherbrand Bead Mill Homogenizer 24 at full speed (6 m/s) for two 23-second cycles. If the samples were not thoroughly homogenized, the cycle was repeated after a 5-minute pause. This IDEXX EIA method uses selective antigen-antibody binding in a seprion ligand-coated 96-well plate by adding 100 µL of buffered samples (BHs) in duplicate into each well. This was followed

by incubation at room temperature for 45-60 minutes with agitation (200±100 rpm), and three washes with a wash buffer to remove unbound BH.

Next, 100 µL of conditioning buffer was added to each well, and the plate was sealed and incubated for 10 ± 1 minutes. Then, an enzyme-linked secondary antibody, the conjugate, was introduced. The plate was incubated for 45 minutes to allow the conjugate to bind to the captured antigen. After another wash, 100 µL of 3,3',5,5'-Tetramethylbenzidine (TMB) substrate was added to each well. The plate was incubated in the dark for 15 ± 1 minutes to enable colour development. Next, 100 µL of acid stop solution (1 M HCl) was added to stop the reaction. Absorbance readings were then taken, and the colour intensity, which reflects the quantity of the target protein, was measured using a BioRad IMark plate reader at 450 nm with a reference wavelength of 620-650 nm. Each plate of the individual IDEXX run included additional internal negative and positive controls to monitor the performance and variability of each run compared to others.

2.3.2. Evaluating NfL Levels in the Brain Using CSF NF-Light ELISA

Similarly, NfL levels in different regions of the CNS of BSE-challenged animals (C-, H-, and L-type; n = 3) and controls (n = 3) were measured using Quanterix Human NF-Light ELISA kit for CSF (Uman Diagnostics, 10-7002-RUO), which employ an antibody-coated 96-well plate and the same samples described for the IDEXX EIA were tested. The assay involved preparing a series of standard solutions ranging from 125 to 5000 pg/mL using the provided diluent. These standards were tested alongside the samples on the same plate. The protocol recommended only a 2-fold dilution; however, this proved ineffective due to species- and sample-specific variation (e.g., brain tissue instead of CSF), and the NfL reading exceeded the kit's detection limit. Samples were diluted multiple times over a

broad range (3000-9000-fold), as NfL levels were extremely high and highly variable across brain regions.

The 96-well plates, pre-coated with a human anti-NfL antibody, were pre-washed with the provided buffer using the QUANTX 3 program incorporated in the BioRad plate washer, applying 300 µL of buffer to each well three times. Following this, 100 µL of diluted standards and samples were added to their designated wells in duplicates and incubated for 1 hour at room temperature with agitation set at 800 rpm.

The plate was rinsed again with wash buffer before adding 100 µL of freshly diluted tracer antibody to each well. The plate was sealed and incubated at room temperature for 45 minutes with agitation. After another round of washing, each well received 100 µL of freshly diluted conjugate. The plate was sealed and incubated for 30 minutes at room temperature with agitation, followed by a final wash, and then 100 µL of TMB substrate was added to each well. The plate was sealed and incubated for 15 minutes at room temperature in the dark with constant agitation. The provided stop reagent (STOP; 50 µL) was added to each well to terminate the reaction. Absorbance was then measured at 450 nm with a 620 nm background correction, ensuring that the absorbance of the 5000 pg/mL standard was above 2.0 AU, and the background absorbance was below 0.1 AU for the assay to be valid. The plate reader was programmed to calculate optical density and NfL concentration (pg/mL) using the formula provided in the kit insert. Concentrations were automatically determined using NF-Light Human CSF ELISA kits and immunoassay software employing a $1/y^2$-weighted 4-parameter algorithm to yield the best fit. The actual concentrations were then calculated, accounting for all dilutions, using the following formula, where c stands for concentration and v is for volume:

$$c_1 v_1 = c_2 v_2$$

Therefore, final cumulative results for NfL readings were gathered from separate runs, with inter-plate controls used in all runs and controls evaluated across runs to check for any variation. A control track chart was created to monitor assay performance each time by recording the controls' results.

2.3.3. Analysis of PrP^{Sc} and NfL Levels in the Brain Using Immunohistochemistry (IHC)

Seven brain regions from each of the twelve animals were prepared to examine the relationship between PrP^{Sc} deposition and NfL regulation in BSE. These tissues were previously fixed in formalin and embedded in paraffin at the time of collection to preserve them. Brain tissues from each animal were sliced into three consecutive sections, each 4 microns thick, to eliminate within-animal variation and prevent experimental bias. For validation of IHC staining, the experiments were designed with three different treatment conditions per tissue section: (1) no primary antibody (antibody control), (2) anti-PrP F99 antibody (for PrP^{Sc} deposition), and (3) anti-NfL 2F11 antibody (for NfL regulation).

Each experiment was deemed successful if the no-primary-antibody control showed no staining. Additionally, for PrP^{Sc} staining, brain tissues from a known BSE-negative and a positive animal served as controls, respectively, and were included in each run to assess staining. Similarly, for NfL staining, the positive control consisted of brain tissue from BSE-positive animals. Conversely, jejunum (intestinal tissue being a non-CNS tissue) from a positive BSE animal was used as the negative control. The presence of controls confirmed that any bound antibodies correctly attached to antigens and that there was no non-specific labelling. In this way, nearly 252 slides were stained in total.

Each IHC experiment began by deparaffinizing the tissue slides by placing them in an oven at 58 ± 4 °C overnight or for at least 1 hour before staining. The tissue sections were hydrated on an automated stainer, then subjected to 10 dips in Milli-Q water to remove excess chemicals. The slides were then incubated in 3% hydrogen peroxide for 10 minutes to inhibit endogenous peroxidase and prevent nonspecific staining. This was necessary to expose the antigen that may be masked during tissue fixation; the tissues were placed in Milli-Q water. Additionally, all slides were treated with 99% formic acid for 5 minutes to reduce prion infectivity. Following this, the washed sections were treated with 100 mM Tris buffer (pH 7.6) for 3 minutes, then washed for 5 minutes to stabilize the tissue's pH for binding. Then, the slides were placed in the autoclave at 125 °C for 1 hour to perform antigen retrieval. Once cooled to room temperature, the slides were transferred to Shandon units for incubation, which were then washed with TBST (Tris-buffered saline) for 5 minutes and incubated with 100 µL of 5 % normal goat serum for 15 minutes, serving as a blocking solution to prevent nonspecific staining. 100 µL of primary antibodies was added, and the slides were incubated overnight. For PrP^{Sc} detection, tissue sections were incubated with F99 (mouse monoclonal anti-PrP, clone F99/97.6.1, VMRD, USA) (1:18000) diluted in TBST buffer.

To detect NfL, the commonly used anti-mouse antibodies 2F11 (mouse monoclonal anti-NfL, M0762, Agilent Technologies/Dako, Denmark) and MS1(mouse monoclonal, LS-C39197, Lifespan Biosciences, USA), were evaluated, as similar antibodies are widely used for neurofilament light chain detection in mammalian systems [28, 57]. Various trials were conducted to optimize NfL capture with these antibodies across different dilutions. For 2F11, dilutions of 1:50, 1:100, 1:200, 1:400, and 1:800 were tested, while MSI was

assessed at no dilution, 1:2, 1:10, and 1:20. With the help of a pathologist, it was concluded that the 2F11 antibody at a 1:200 dilution produced the best results for visualizing NfL in the brain, based on its specificity and clear labelling with minimal background staining.

The following day, two TBST washes were conducted for 5 minutes each to remove unbound antibody. The staining process was then completed with a 30-minute incubation in 100 µL of an HRP-conjugated secondary anti-mouse antibody (DAKO EnVision+ System-HRP-labelled polymer anti-mouse, K4001, Agilent Technologies Denmark). Afterwards, the tissues were developed with fresh 3,3'-Diaminobenzidine (DAB) for 5 minutes. DAB interacts with the peroxidase-conjugated secondary antibody, resulting in a brown colour at the site of the target antigen within the tissue. After DAB, the slides were stained with hematoxylin for 45 seconds. Next, they were blued with lithium carbonate for 1 minute. Once finished, the slides were dehydrated, coverslips were placed using mounting media (Micromount Mounting Medium,3801730, Leica), and the slides were allowed to dry for 24-48 hours.

IHC quantification was performed by capturing images of all stained tissues using ZEN 3.4 software with an Axiocam 712 colour camera on a light microscope (ZEISS). All images were captured at 40x to produce high-resolution, detailed images. For each section, three random fields were captured to ensure a representative sample of the tissue's location. Settings were kept consistent to prevent variation. Therefore, the display settings were configured to RGB with low contrast and auto-exposure to ensure uniform illumination. Image acquisition was set to 24-bit depth, with the inner region of interest (ROI) maintained at 4096 x 3008 pixels. A 3x3-pixel binning was set to 1x1, with binning-independent brightness enabled to keep uniform brightness across pixels. The captured frames had dimensions of 767 x 563 pixels, scaled to 18.43 x 18.43 pixels, resulting in images of

14138.87 x 10377.60 pixels. Images were exported as TIFF to preserve high quality and fine details. All captured images for each sample across all animals are available in the supplementary materials.

Processing of those images was carried out using Fiji (Fiji Is Just ImageJ), an open-source image analysis platform, following the colour deconvolution protocol described in [58]. This step involved adjusting the image threshold and selecting the colour channel designated for DAB staining, which separates the brown staining from the rest of the image. Following this, the threshold was optimized until all accurate brown signals were captured by adjusting the slider on the scaling bar. Once the threshold was determined, the images were converted to binary by assigning white and black colours and setting all selected brown-staining pixels to white. In contrast, the background was transformed into black pixels. Then, the watershed algorithm was applied to separate any fused or overlapping cells. Next, numerical data were obtained by extracting the shaded intensity, providing mean grey values along with the minimum and maximum intensity (Supplementary Figure 1).

Those measurements were transformed into relative optical densities using the following formula:

$$\mathrm{Log}\left(\frac{\text{Maximum Intensity}}{\text{Mean Intensity}}\right)$$

These thresholds aim to enable the selection of the signal of interest and the removal of background noise. This was especially important because the negative controls exhibited intense background for anti-PrP staining. It is worth noting that slides from negative control animals underwent a post-mortem examination many years ago, after which they were found to be negative; however, ImageJ captured signals that were only visible in the

software, not to the naked eye. Consequently, different thresholds were tested and applied to only two groups: the negative control and C-BSE. The three thresholds used in those trials are as follows: (0-175), (0-200), and (0-217) (Supplementary Figure 2). The middle range (0-200) yielded the best results among the three options. It allowed for the detection of accurate signals with minimal background interference. The other two ranges were either too low or too high, producing larger error bars or excluding actual signals.

Optimization was also needed to process and quantify the signal resulting from anti-NfL primary antibody 2F11 staining. The thresholds were tested at three intervals: (0-150), (0-175), and (0-200) (Supplementary Figure 3). Meanwhile, the 0-175 range was most effective for isolating the NfL-specific signal from the background.

Once the thresholds for PrP^{Sc} and NfL signals were optimized, they were applied to the remaining images for other BSE groups. The quantification was performed by maintaining consistent thresholds within and between brain regions and animals. The average optical densities were calculated for all three frames of each brain tissue sample to ensure accuracy and consistency.

2.3.4. Evaluating NfL Levels in CSF Using CSF NF-Light ELISA

NfL levels in the CSF were quantified using the CSF NF-Light ELISA kits, following the manufacturer's instructions. They were performed as described above for brain tissues, with a slight modification to the dilution. An optimization experiment was conducted to determine the optimal dilution for CSF samples from BSE-positive and negative animals (supplementary figure 4). A total of seven animals were tested in the optimization experiment: two from each BSE group and only one L-BSE sample. Along with negative controls, they were tested at four different dilutions: 1:2, 1:4, 1:10, and 1:20.

Based on the optimization experiment, a 1:2 dilution was identified as optimal for BSE-negative samples to achieve lower detection limits of the kit, whereas a 1:20 dilution was selected for BSE-positive samples to prevent readings exceeding the upper detection limit of the kit. For determining NfL levels in CSF, a total of 13 CSF samples were used, comprising n=4 for controls, n=5 for C-BSE, and n=2 for each of L-BSE and H-BSE. The test was repeated twice to ensure accuracy and reproducibility. The results were averaged over two runs and analyzed to determine NfL concentration in the CSF sample. The intra-assay coefficient of variation (CV%) for cerebrospinal fluid (CSF) samples ranged from 0.256% to 6.671% across all standards and assay runs. Most CV values were below 3%, indicating high repeatability and strong analytical precision within individual runs. Only a small number of measurements approached approximately 5–6%, which remains within acceptable limits for immunoassay performance. Overall, these results demonstrate good intra-assay precision and reliability of the assay for CSF NfL quantification; meanwhile, inter-assay variability, including variation between different kit lots, was monitored using internal control tracking chart. Control values across all runs remained within ±2 SD of the mean, demonstrating consistent assay stability over time (Supplementary Figure 6). Then, the specificity and sensitivity of NfL in CSF were assessed using Receiver Operating Characteristic (ROC) analysis.

2.3.5. Evaluating NfL Levels in Clinical Blood Using Serum NF-Light ELISA

A total of 15 blood samples were analyzed. The assay was performed according to the manufacturer's instructions for the Human NF-Light Serum ELISA Kits. These samples were collected at the clinical stages of the disease, which may have varied slightly among animals. At least three biological replicates were included for each of the four types of

animal groups. For testing, serum samples were reconstituted in ELISA diluent according to the manufacturer's guidelines. A dilution series of the standard, ranging from 0 to 40 pg/mL, were prepared and used only fresh. Negative and positive inter-plate controls were included on each plate to monitor their performance and track variation from experiment to experiment.

Before conducting a comprehensive experiment on all samples, a pilot experiment was performed to analyze the optimal dilution for bovine serum samples. Previous studies have shown that NfL levels in prion samples from sheep and humans can be as high as ~296 pg/mL and 75.3 ± 15.7, respectively. In contrast, healthy controls showed significantly lower levels, ranging from ~7 to 14.5 pg/mL in humans and from ~12.5 pg/mL in sheep [59, 60]. Those serum kits recommend using four-fold dilutions, which would give a detection range of 1-25 pg/mL or (4-100 pg/mL in the undiluted samples). During preliminary experiment design, differences in NfL levels among species were considered, along with the possibility that BSE samples could fall outside the assay detection limits. Therefore, three dilutions (1:2, 1:4, and 1:8) were selected to account for samples with low, moderate, and high NfL concentrations (Supplementary Figure 5).

Six serum samples were used for this optimization test, consisting of two C-BSE, two H-BSE, and two L-BSE. When the serum samples were diluted 1:2 and 1:4, some samples exceeded the assay's maximum detection limit. However, a 1:8 dilution produced results within the validated range (1–25 pg/mL) for all animals. Therefore, 1:8 was chosen as the optimal dilution for the remaining experiments. After this optimization, all 15 available bovine serum samples were diluted 8-fold, comprising three negative controls, six C-BSE, three H-BSE, and three L-BSE.

First, the wells were pre-washed (3x 300 µL of 1X Wash buffer) using the Quanterix 3. Diluted samples, standards, and blanks, along with inter-plate controls, were loaded in duplicate (200 µL per well), followed by incubation for 2 hours at room temperature on a shaker at 800 rpm.

At the end of incubation, the plate was washed using the same program. 100 µL of the detector antibody was added to each well, and the wells were incubated for 90 minutes with shaking. This was followed by washing and incubation with 100 µL of conjugate for 30 minutes. After incubation, the plate was washed with Quanterix 6 (6 x 300 µL), and 100 µL of TMB substrate was added to each well for 15 minutes; the reaction was then stopped by adding 50 µL of Stop solution.

Plates were read at 450 nm with 620 nm background correction, and NfL concentrations were interpolated as described previously. Validity criteria included: blank optical density (OD) < 0.25 AU, calibrators within defined ranges, and the top standard signal exceeding 2.0 AU. The intra-assay coefficient of variation (CV%) for blood samples ranged from 0% to 8.53% across all standards and assay runs. Most CV values were below 5%, indicating high repeatability and acceptable analytical precision within individual runs and inter-assay variation was assessed similarly to that described for CSF (Supplementary Figure 6). Subsequently, ROC analysis was an experimental part, like 2.3.4

2.4. Evaluation of NfL Stability in CSF and Serum

For both CSF and serum, the effect of freeze-thaw was first assessed by aliquoting samples and storing them at ~-80 °C. A total of three positive C-BSE samples were tested. On day one, these samples were retrieved from the -80 °C freezer and thawed, marking the completion of cycle one; each cycle began at the time of freezing and was considered

complete upon thawing. Cycle one served as the starting point, and for each sample, three identical aliquots were prepared for evaluation at cycles 1, 5, and 10. Those from cycle one were stored until the testing day. For five and ten cycles, the process was conducted over two days: each aliquot was frozen at approximately -73 °C for 1 hour, then thawed at room temperature (~22 °C) in the lab, with time and temperature recorded for each cycle. On day one, 4.5 cycles were completed for the 5-cycle target samples, which were then stored until testing. For the 10-cycle samples, 9.5 cycles were completed by the second day, using the same approach of alternating freezing and thawing for 1 hour each. On the third day, all samples were removed from the freezer and tested together on the same plate using Quanterix NfL ELISA kit for either CSF or serum, respectively, as per the manufacturer's instructions described above.

The same three positive BSE animals were used to evaluate NfL stability at different storage temperatures. This process took place over 10 days and involved testing CSF and serum samples at room temperature (~22 °C), at ~5 °C for 5 and 10 days, and at -80 °C, which served as the baseline. Five identical aliquots of each sample were prepared: one was stored at room temperature (~22 °C), at 5°C, and another at -80°C for the entire ten days, starting on day 1. On day 5, a second set of aliquots of each sample was placed at room temperature and at ~5°C until day 10. Daily temperature readings were taken for both the room and the fridge, with the days listed in ascending order. The samples from all three temperature points and durations (5 days or 10 days) were assessed on day 11 on the same plate using Quanterix NfL ELISA kit for either CSF or serum, respectively.

2.5. Statistical Data Analysis

The outputs from all three aims were initially assessed visually using bar graphs and then tested for normality and homogeneity of variances. Histograms showed widely dispersed values with no prominent peak, confirming a non-normal distribution and violating the assumptions of parametric tests, such as ANOVA [61]. Levene's test [62] revealed heterogeneity of variances, consistent with the small sample size as reflected in the descriptive analysis (mean ± SEM). Consequently, nonparametric tests were used throughout the study with exact p-values were calculated using GraphPad Prism and reported in tables for each aim. Those tests included Mann Whitney test for comparison among two group, while Kruskal Wallis test for more than two groups comparison ad Spearman correlation was used to assess any potential association. Additional, ROC analysis was automatically computed and performed by GraphPad prism which gave area under curve (AUC), p values, specificity, sensitivity and cut off for differentiation among groups.

3. Results

3.1.1. Analysis of Correlation Between PrP^{Sc} and NfL Levels in the Brain Using ELISA

Analysis of PrP^{Sc} and NfL levels and their potential correlation in different regions of the CNS of various types of BSE was performed by using two approaches: i) ELISA and ii) IHC. The IDEXX EIA performed for determining the presence of PrP^{Sc} indicated high levels of PrP^{Sc} throughout the brains of all BSE animals (Figure 1). The mean OD values representing the relative presence of PrP^{Sc} showed a trend of higher PrP^{Sc} amounts in frontal cortex and thalamus, and low PrP^{Sc} amounts in occipital cortex, cerebellum hemisphere and cerebellum peduncle in C- BSE animals compared to H- and L-type BSE. Interestingly, PrP^{Sc} quantities in the obex regions of the brain in all types of BSE animals were indistinguishable. On the contrary, mean OD values in all areas of the brains of control animals were closer to zero, indicating no relative amount of PrP^{Sc}. Overall, all BSE-positive animals showed significantly higher PrP^{Sc} levels, clearly distinguishing them from controls.

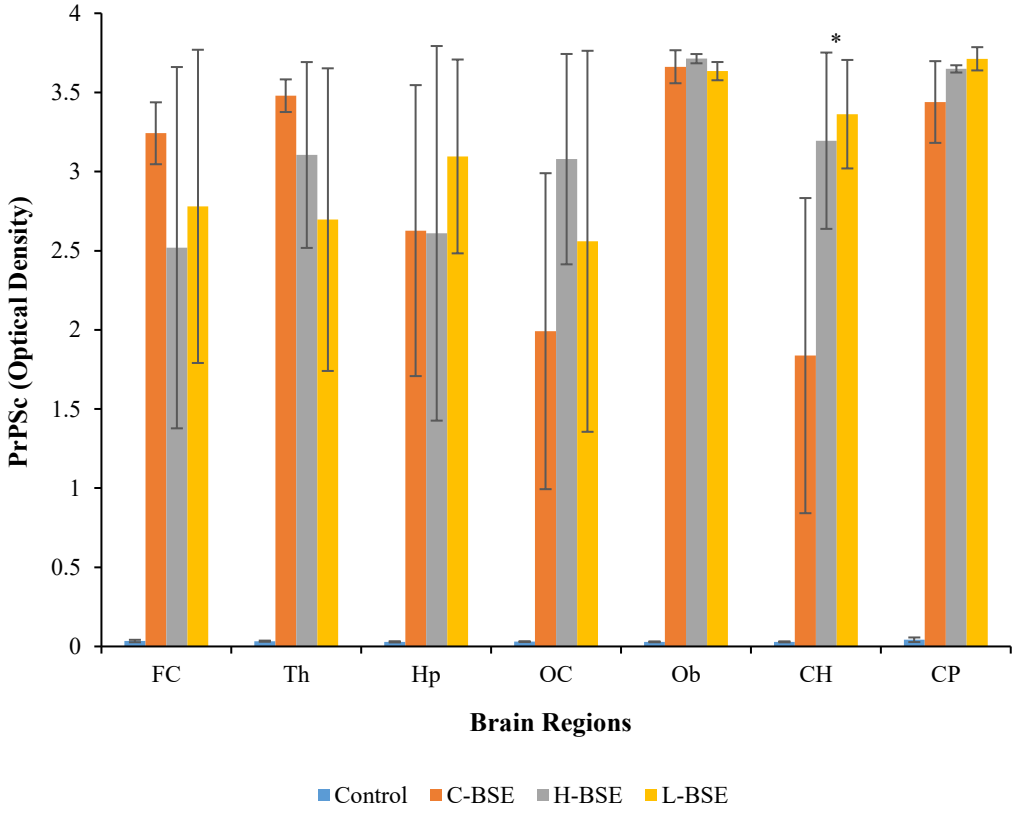

Figure 1: IDEXX EIA results indicating the presence of PrP^{Sc}. Mean ± SEM of optical density (OD) values representing the relative abundance of PrP^{Sc} in seven regions of the CNS in C-BSE, H-BSE, L-BSE, and control animals, including frontal cortex (FC), thalamus (Th), hippocampus (Hp), occipital cortex (OC), obex (Ob), cerebellar hemisphere (CH), and cerebral peduncle (CP). Each point represents the mean of n = 3 animals, except for the hippocampus in C-BSE (n = 2), with $p < 0.05$ (*).

On the other hand, NfL concentrations were measured in all four groups and varied across regions, with the lowest values in the frontal cortex and the highest near the obex (Figure 2). NfL levels were indistinguishable between healthy controls and positive-BSE strains, with levels similar in some cases, lower in others, and even higher in some strains, with no consistent trend across the four groups. Overall, all four groups exhibit a considerable level of NfL, with results not being statistically significant across most tissues ($p > 0.05$).

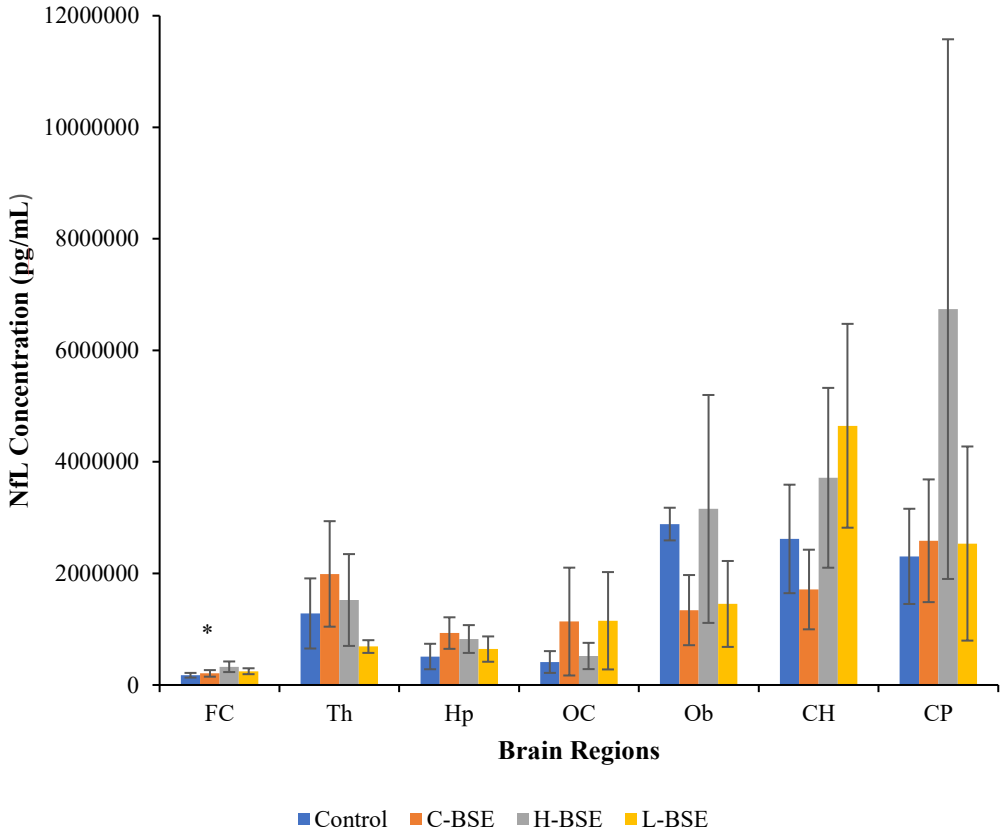

Figure 2: CSF Nf-Light results showing NfL levels. Mean ± SEM of dilution-corrected NfL concentrations (pg/mL) across seven regions of the CNS in C-BSE, H-BSE, L-BSE, and control animals, including frontal cortex (FC), thalamus (Th), hippocampus (Hp), occipital cortex (OC), obex (Ob), cerebellum hemisphere (CH), and cerebral peduncle (CP). Each point represents the mean from n = 3 animals per group, except for the hippocampus in C-BSE (n = 2), with $p < 0.05$ (*).

ELISA results for PrP^{Sc} and NfL across all seven brain regions in the four experimental animal groups showed variability, as indicated by large SEM bars. To assess significance among the four groups shown in Figures 1 and 2, the Kruskal-Wallis test was performed; the results are shown in Table 2. No consistent statistical significance was found across regions for the levels of both PrP^{Sc} and NfL between BSE positive and control animals.

Table 2: Kruskal-Wallis H-statistics and their corresponding exact p-values for PrP^{Sc} and NfL levels measured by ELISA in the CNS. Seven brain regions were analyzed, including the frontal cortex (FC), thalamus (Th), hippocampus (Hp), occipital cortex (OC), obex (Ob), cerebellum hemisphere (CP), and cerebral peduncle (CP). The study included four groups (n=3 each): negative control, C-BSE, H-BSE, and L-BSE.

Brain Regions	**FC**	**Th**	**Hp**	**OC**	**Ob**	**CP**	**CH**
H-Statistic PrP^{Sc}	6.590	6.282	6.258	6.590	6.897	7.205	6.692
P	0.0681	0.0850	0.0738	0.0681	0.0502	0.0382	0.0599
H-Statistic NfL	2.692	0.744	1.879	0.436	2.077	2.487	0.4359
P	0.0488	0.9006	0.6552	0.9586	0.6098	0.5312	0.9586

To improve clarity, comparisons were reduced to two groups: all BSE types (n = 9) versus the control (n = 3), as shown in Figures 3 and 4. When all three BSE strains were combined, PrP^{Sc} was most concentrated in the obex and cerebellar peduncle, followed by the thalamus, then the frontal cortex, and finally the hippocampus and occipital cortex, with increased statistically significant differences.

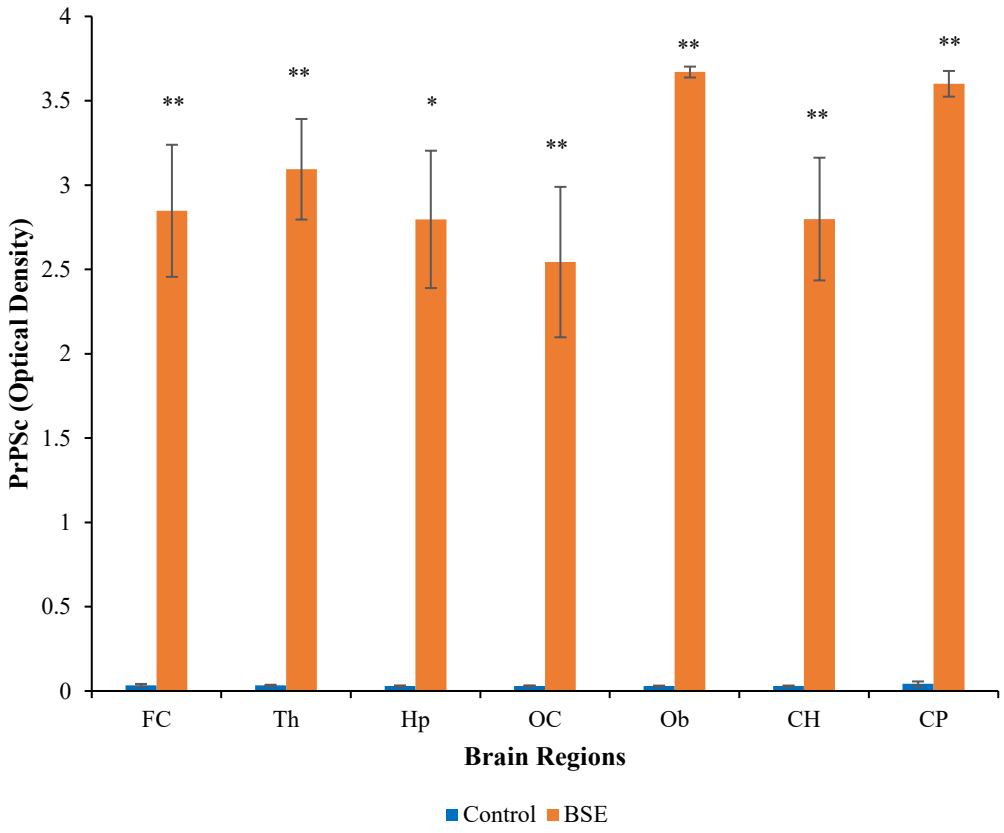

Figure 3: Mean ± SEM of optical densities for PrP^{Sc} across seven regions of the CNS in all BSE-positive animals combined (n=9) versus healthy controls (n=3). Levels were measured in frontal cortex (FC), thalamus (Th), hippocampus (Hp), occipital cortex (OC), obex (Ob), cerebellum hemisphere (CH), and cerebral peduncle (CP) using IDEXX EIA, with $p<0.05$ (*) and $p<0.01$ (**).

For NfL analysis, when all BSE types were combined, NfL levels were generally higher in BSE-positive samples across most brain regions, except at the obex, where NfL levels were lower than in controls. Still, the difference in obex between BSE and control animals was not statistically significant ($p > 0.05$).

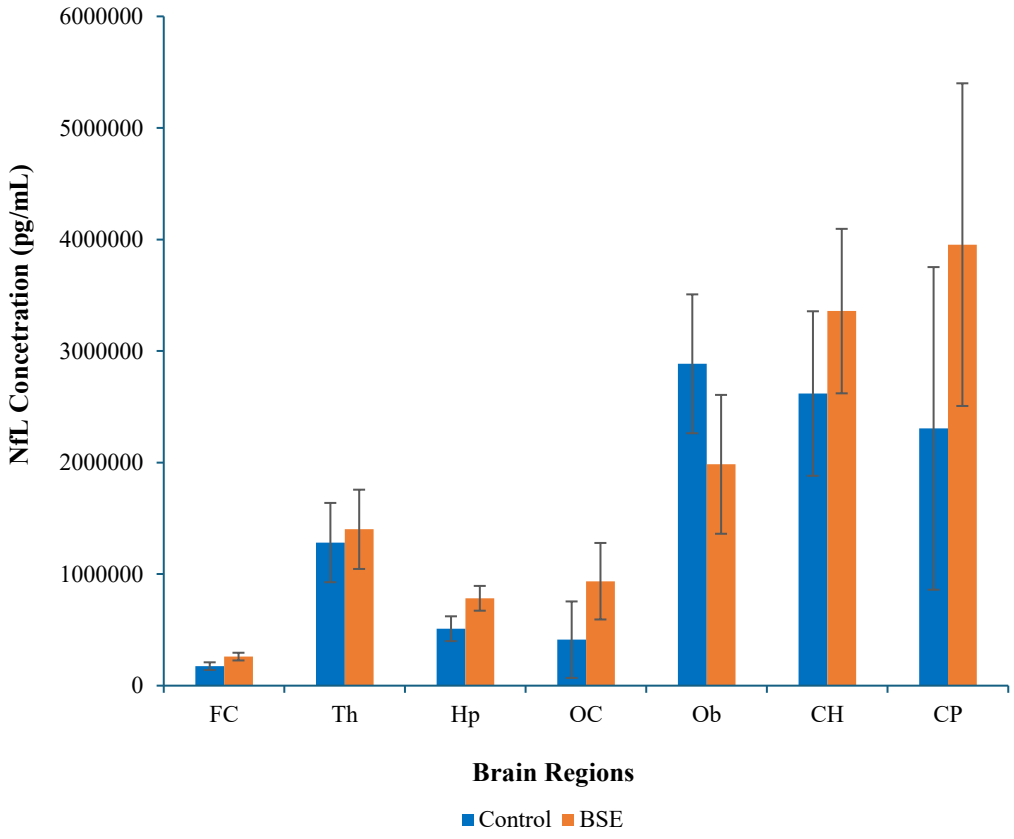

Figure 4: Mean ± SEM of NfL-dilution-corrected concentrations in pg/mL across seven regions of the CNS in all BSE-positive animals combined (n=9) versus healthy controls (n=3). Levels were measured in the frontal cortex (FC), thalamus (Th), hippocampus (Hp), occipital cortex (OC), obex (Ob), cerebellum hemisphere (CH), and cerebral peduncle (CP) using the CSF-NF-Light kit, and p-values were >0.05 in all regions.

The Mann-Whitney test results for the two-group comparison shown in Figures 3 and 4 are presented in Table 3 below, indicating that PrP^{Sc} levels differed significantly between negative and positive BSE animals, whereas NfL levels did not.

Table 3: Mann-Whitney U-statistics and exact p-values for PrP^{Sc} and NfL levels measured by ELISA in the CNS. Levels were measured in seven brain regions in two groups: negative BSE (n=3) and positive BSE animals (n=9).

Brain Regions	**FC**	**Th**	**Hp**	**OC**	**Ob**	**CH**	**CP**
U-Statistics PrP^{Sc}	0	0	0	0	0	0	0
P	0.0091	0.0091	0.0121	0.0091	0.0091	0.0091	0.0091
U-Statistics NfL	8	13	7	12	6	11	12
P	0.3727	> 0.99	0.3758	0.8636	0.2091	0.7273	0.8636

Based on ELISA results for PrP^{Sc} and NfL in BSE-positive animals, a correlation analysis was performed by calculating the correlation coefficients (ρ) between PrP^{Sc} optical density and NfL concentration (pg/mL) in each brain region (Figure 5). Correlation coefficients varied across all seven brain regions, with the hippocampus showing the strongest positive correlation (0.6455), which is moderate. The cerebellar hemisphere (0.5035), frontal cortex (0.4196), thalamus (0.3776), and cerebral peduncle (0.2517) exhibited slightly weaker correlations, while the occipital cortex (0.2587) and the obex (-0.2797) displayed a weak negative correlation. Overall, no statistically significant relationships were identified ($p > 0.05$), except in the hippocampus, suggesting a limited association between these two biomarkers in this dataset.

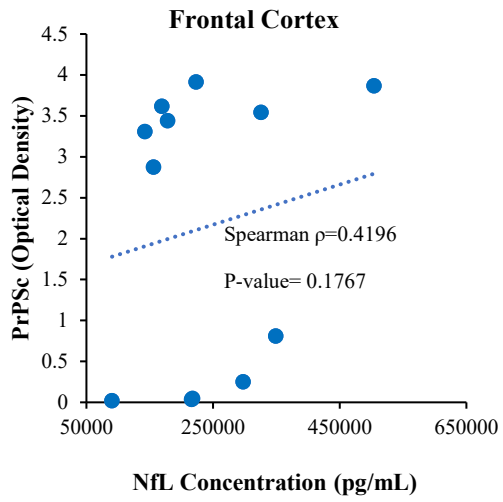
Frontal Cortex
PrPSc (Optical Density)
NfL Concentration (pg/mL)
Spearman ρ=0.4196
P-value= 0.1767

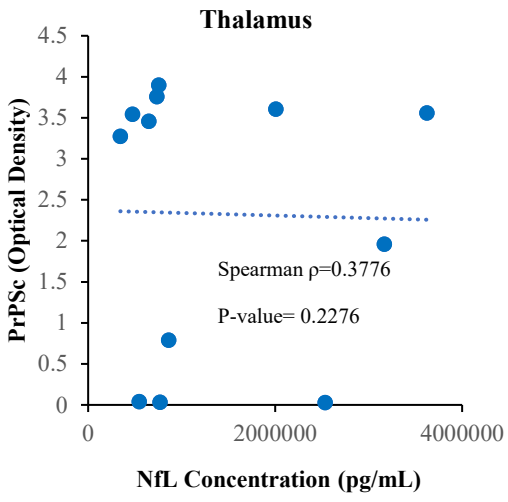
Thalamus
PrPSc (Optical Density)
NfL Concentration (pg/mL)
Spearman ρ=0.3776
P-value= 0.2276

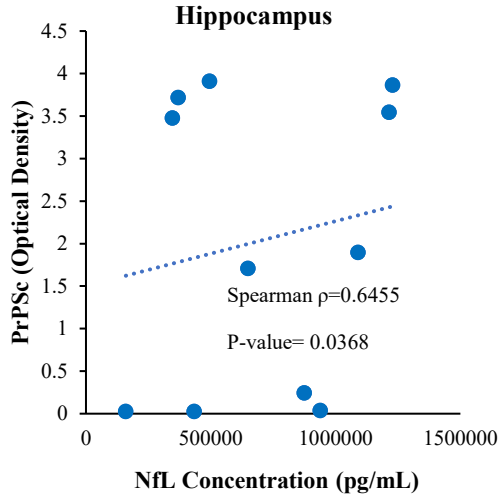
Hippocampus
PrPSc (Optical Density)
NfL Concentration (pg/mL)
Spearman ρ=0.6455
P-value= 0.0368

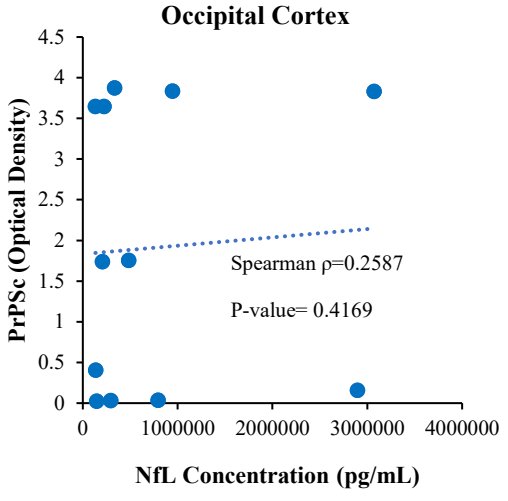
Occipital Cortex
PrPSc (Optical Density)
NfL Concentration (pg/mL)
Spearman ρ=0.2587
P-value= 0.4169

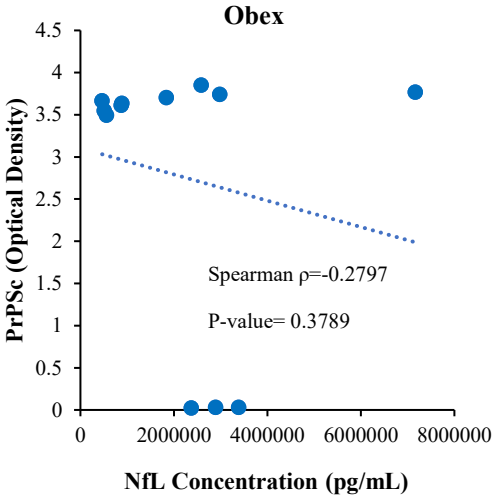
Obex
PrPSc (Optical Density)
NfL Concentration (pg/mL)
Spearman ρ=-0.2797
P-value= 0.3789

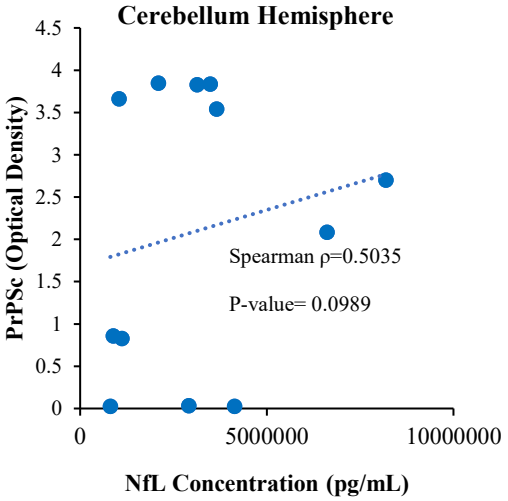
Cerebellum Hemisphere
PrPSc (Optical Density)
NfL Concentration (pg/mL)
Spearman ρ=0.5035
P-value= 0.0989

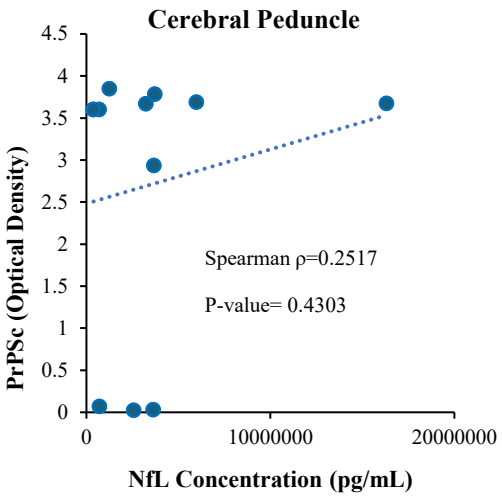

Figure 5: Scatterplot showing the Spearman correlation coefficients (ρ) between the optical density of PrP^{Sc} and NfL concentrations (pg/mL), measured by ELISA, with their exact p-values. Data are shown for seven brain regions: frontal cortex, thalamus, hippocampus, occipital cortex, obex, cerebellum hemisphere, and cerebral peduncle.

3.1.2. Analysis of Correlation Between PrP^{Sc} and NfL in the Brain Using IHC.

To confirm the correlation between PrP^{Sc} and NfL and to extend the ELISA findings, IHC was performed using anti-PrP F99 and anti-NfL 2F11 antibodies across different regions of the CNS of BSE-positive and control animals. Figures 6-11 illustrate the staining and its corresponding quantified signals (relative intensities) for PrP^{Sc} and NfL in various brain regions. IHC revealed that PrP^{Sc} accumulation was specific to each BSE strain and was consistently observed only in BSE-positive animals. Meanwhile, NfL staining showed greater variability and, in some cases, could distinguish between negative and positive animals; however, these differences were not statistically significant.

PrP^{Sc} staining deposits display distinct patterns, with variations between brain regions and strains (Figure 6). As expected, the healthy control showed no PrP^{Sc} immunostaining, whereas the three BSE strains exhibited distinct, intense PrP^{Sc} deposition.

In the C-BSE group, the range varied from minimal in the frontal cortex, with low prion pathology and faint PrP^{Sc} staining, to mild in the thalamus, and moderate to more extensive staining in the hippocampus, including isolated areas. Like the frontal cortex, the occipital cortex also showed low to moderate PrP^{Sc} deposition. The obex exhibited a moderate, scattered prion level, mainly in the central grey matter. The cerebellum showed a moderate localized deposition, while scattered in the cerebral peduncle.

While in H-BSE, the frontal cortex showed a diffuse cluster of prions that were more intense than in C-BSE. The thalamus exhibited a staining intensity similar to that of the hippocampus but was more isolated and slightly stronger in the occipital cortex. The obex displays the most intense staining and indicates the primary pathology across all samples and BSE forms examined, with severe damage and significant staining in both neuronal cell bodies and surrounding tissue, suggesting greater involvement of this region. While the PrP^{Sc} occurs to a lesser extent in the cerebellum hemisphere and cerebellar peduncle, it remains more noticeable than in C -BSE and is more widespread in both grey and white matter.

Conversely, the L-BSE showed low levels of PrP^{Sc}, with faint staining in the frontal cortex, while the thalamus exhibited more intense staining in both cell bodies and surrounding tissue. Immunostaining decreased in the hippocampus and occipital cortex relative to frontal cortex and thalamus and was most prominent at the obex among all regions, although less intense than in H-BSE. The cerebellar hemispheres showed minimal PrP^{Sc}, while the cerebral peduncles displayed PrP^{Sc} throughout the region. These findings suggest that different BSE strains may exhibit distinct PrP^{Sc} staining patterns and spatial preferences for PrP^{Sc} deposition.

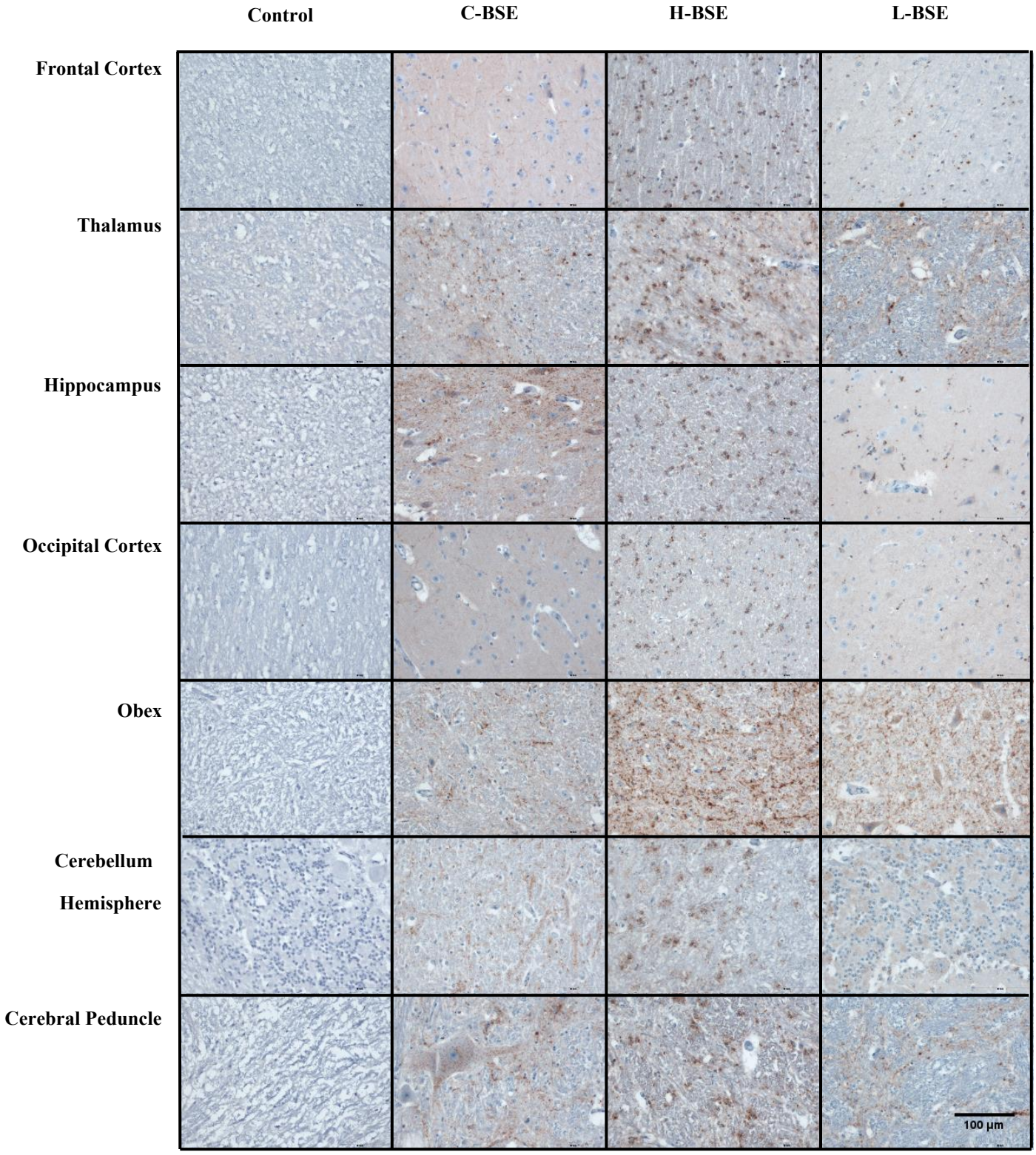
Control
C-BSE
H-BSE
L-BSE
Frontal Cortex
Thalamus
Hippocampus
Occipital Cortex
Obex
Cerebellum
Hemisphere
Cerebral Peduncle
100 µm

Figure 6: IHC staining for PrP^{Sc}, captured at 40X magnification with a 100 μm scale bar. The images show four animal groups, including a negative healthy control, C-BSE, H-BSE, and L-BSE across seven regions of the CNS, each with distinct staining patterns.

IHC quantified signals confirmed the previous ELISA results for PrP^{Sc} levels in the same 12 animals (Figure 7). Consistent with prion findings, control animals showed no signal indicative of PrP^{Sc} deposition, whereas BSE-positive animals exhibited a strong visible signal. In C-BSE animals, PrP^{Sc} was most abundant in the hippocampus, followed by the thalamus and the obex. Moderate PrP^{Sc} deposition was observed in the occipital cortex and cerebellar peduncle, as well as in the frontal cortex and cerebellar hemisphere, compared to controls.

In H-BSE (Figure 7), PrP^{Sc} deposition was most prominent in the thalamus, hippocampus, occipital cortex and obex. On the other hand, moderate PrP^{Sc} deposition was found in cerebellum hemispheres, cerebral peduncles and frontal cortex. In L-BSE, PrP^{Sc} deposits were highest in the hippocampus and obex, followed by the thalamus and cerebral peduncle, and slightly lower in the frontal cortex, with the occipital cortex and cerebellum hemisphere showing the least amount. Overall, L-BSE animals had the lowest PrP^{Sc} deposition compared to C- and H-type BSE in all brain regions. Unfortunately, comparisons of brain regions across all BSE types were statistically significant in only a few areas due to variability in the data.

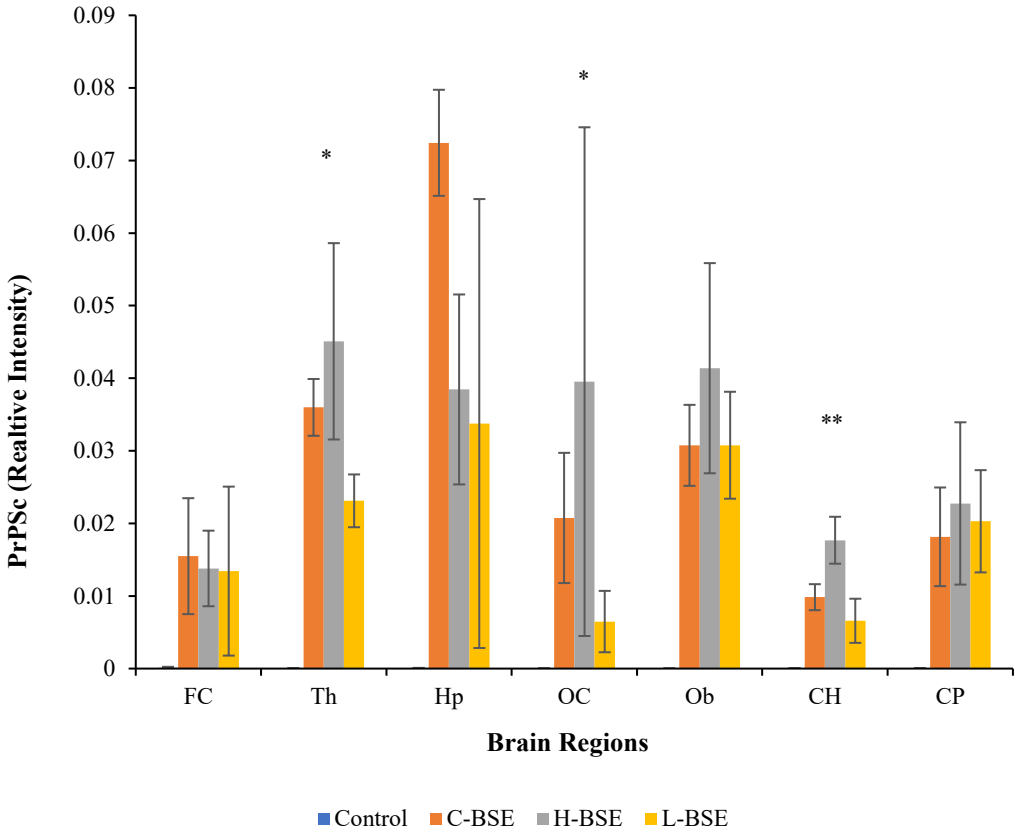

Figure 7: Mean ± SEM of the relative intensity of PrP^{Sc}, obtained by quantifying IHC staining signals, across seven brain regions in C-BSE, H-BSE, L-BSE, and control animals. Brain regions include the frontal cortex (FC), the thalamus (Th), the hippocampus (Hp), the occipital cortex (OC), the obex (Ob), the cerebellar hemisphere (CH), and the cerebral peduncle (CP). Quantification was performed using ImageJ (n = 3 per group), with significance levels of $p<0.05$ (*) and $p<0.01$ (**).

NfL immunostainings were also assessed across various brain tissues in positive BSE animals and negative controls (Figure 8). In the control group, uniform, intact NfL immunolabelling was observed across most regions, including the frontal cortex, with well-defined axonal staining particularly evident in the thalamus and hippocampus. Immunolabelling for NfL showed continuous fibres, indicating a normal and intact NfL distribution, with more intense staining in the occipital cortex but remaining consistent

across regions. The obex showed longitudinal staining without increased density, and the cerebellum hemisphere demonstrated regular NfL presence in the white matter with no aggregated fibres, featuring a more prominent cerebellar peduncle with a standard axon bundle.

Meanwhile, immunostaining in C-BSE was like that in the control group, with a slight increase in the visibility of axonal fibres and some neuronal disruption in certain regions. The frontal and occipital cortices showed mild brown axonal immunostaining, consistent with the control group. While the thalamus and hippocampus exhibited moderate, diffuse neuropil NfL staining, without cluster formation. In contrast, the obex showed clear axonal staining. The cerebellar hemisphere showed enhanced fibre immunostaining within the white matter tracts, with more distinct immunostaining in the cerebellar peduncle.

While H-BSE showed a more widespread pattern of NfL immunostaining across the four groups, both the frontal and occipital cortices exhibited intense, coarse brown axonal immunolabelling. The thalamus and hippocampus displayed noticeable neuropil density. The obex showed strong, widespread reactivity in both white and grey matter. The cerebral hemisphere also demonstrated prominent immunoreactivity in the white matter and fibre tracts, with the cerebral peduncle showing stronger immunostaining, particularly in the fibres.

Conversely, L-BSE showed moderate immunoreactivity for NfL across all tissues, slightly higher than C-BSE and, in some cases, lower than controls, yet still below H-BSE. Moderate, evenly distributed NfL was detected in both cortices, with clear fibre labelling observed in the thalamus and hippocampus at moderate levels. Increased NfL immunostaining was seen in the obex and was mild in both cerebral hemispheres and the

cerebral peduncle. In summary, NfL immunostaining was similar across groups, at least to the naked eye, with some cases showing noticeable differences.

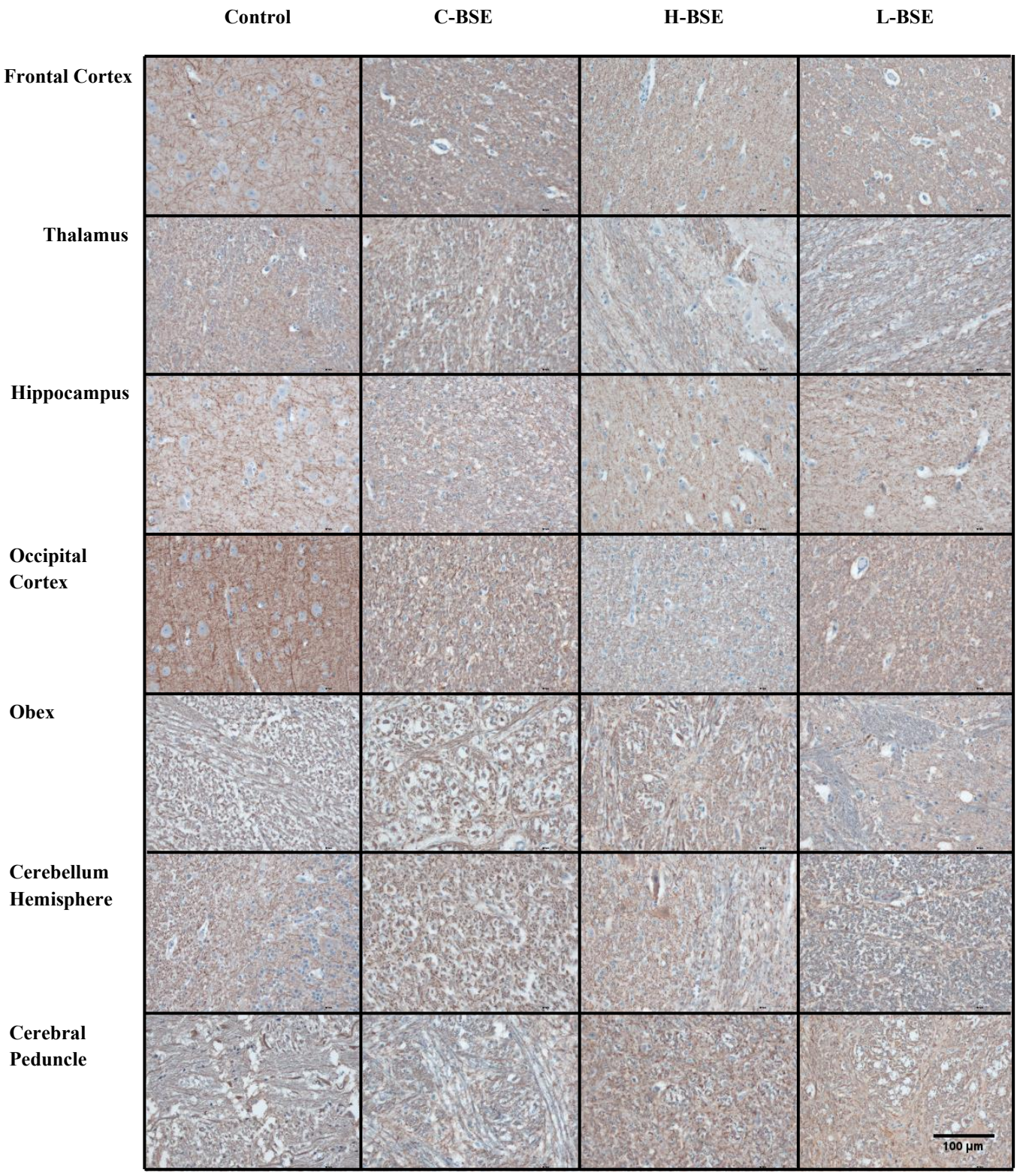

Figure 8: IHC staining for NfL, captured at 40X magnification, with a 100 µm scale bar. The images show four animal groups, including a healthy negative control, C-BSE, H-BSE, and L-BSE, across seven regions of the CNS, each with distinct staining patterns.

The observed immunolabeling trends appeared consistent with the quantified signals; NfL varied among groups (Figure 9). Immunoreactivity with the anti-NfL antibody in BSE-positive and control animals showed differences in NfL distribution across brain regions. Overall, the most prominent pattern is that NfL tends to be lower in most positive BSE cases than in controls, except for a few instances. Due to higher variability among samples, no significant differences were detected.

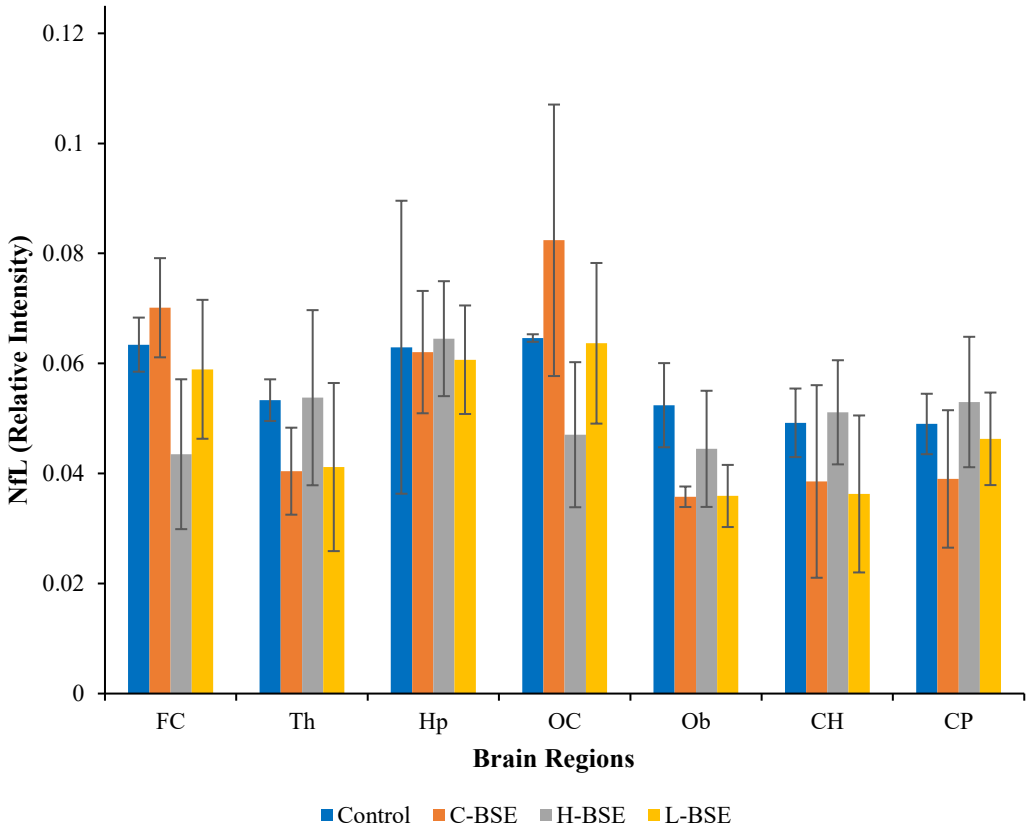

Figure 9: Mean ± SEM of the relative intensity of NfL, obtained by quantifying IHC staining signals across seven brain regions in C-BSE, H-BSE, L-BSE, and control animals. Brain regions include the frontal cortex (FC), the thalamus (Th), the hippocampus (Hp), the occipital cortex (OC), the obex (Ob), the cerebellar hemisphere (CH), and the cerebral peduncle (CP). Quantification was performed using ImageJ (n = 3 per group), with $p > 0.05$ in all tissues.

Following ELISA, IHC was conducted, and the same statistical workflow was used. Bar graphs with SEM showed variability consistent with the ELISA trend. Analysis using the Kruskal-Wallis test for groups shown in graphs 7 and 9 revealed significant differences in PrP^{Sc} levels across the thalamus, occipital cortex, and cerebellar hemisphere; however, pairwise comparisons of PrP^{Sc} did not reach statistical significance. However, in the NfL staining, the difference was not statistically significant (Table 4).

Table 4: Kruskal-Wallis H-statistics and their corresponding exact p-values for PrP^{Sc} and NfL levels, quantified from IHC staining signals in the CNS. Seven brain regions were analyzed, including the frontal cortex (FC), thalamus (Th), hippocampus (Hp), occipital cortex (OC), obex (Ob), cerebellum hemisphere (CP), and cerebral peduncle (CP). The study included four groups (n=3 each): negative control, C-BSE, H-BSE, and L-BSE.

Brain Regions	**FC**	**Th**	**Hp**	**OC**	**Ob**	**CH**	**CP**
H-Statistics PrP^{Sc}	4.538	6.985	5.545	7.076	6.527	8.929	6.235
P	0.2272	0.0382	0.1208	0.0408	0.0707	0.0042	0.0865
H-Statistics NfL	2.282	1.409	0.164	1.513	3.923	0.846	0.539
P	0.5705	0.7551	0.9841	0.7297	0.3040	0.8759	0.9349

For a more comprehensive assessment of overall IHC results, it was necessary to evaluate the output when all BSE strains were grouped (n = 9) and compare it to the control (n = 3), as shown in Figures 10 and 11.

The quantification of PrP^{Sc} signal indicated that PrP^{Sc} was not detected in healthy control animals and was present in BSE-positive animals only (Figure 10). The PrP^{Sc} aggregates were most concentrated in the hippocampus, followed by the thalamus and obex, then in the occipital cortex and cerebral peduncle, with the frontal cortex and cerebellum showing the weakest immunostaining.

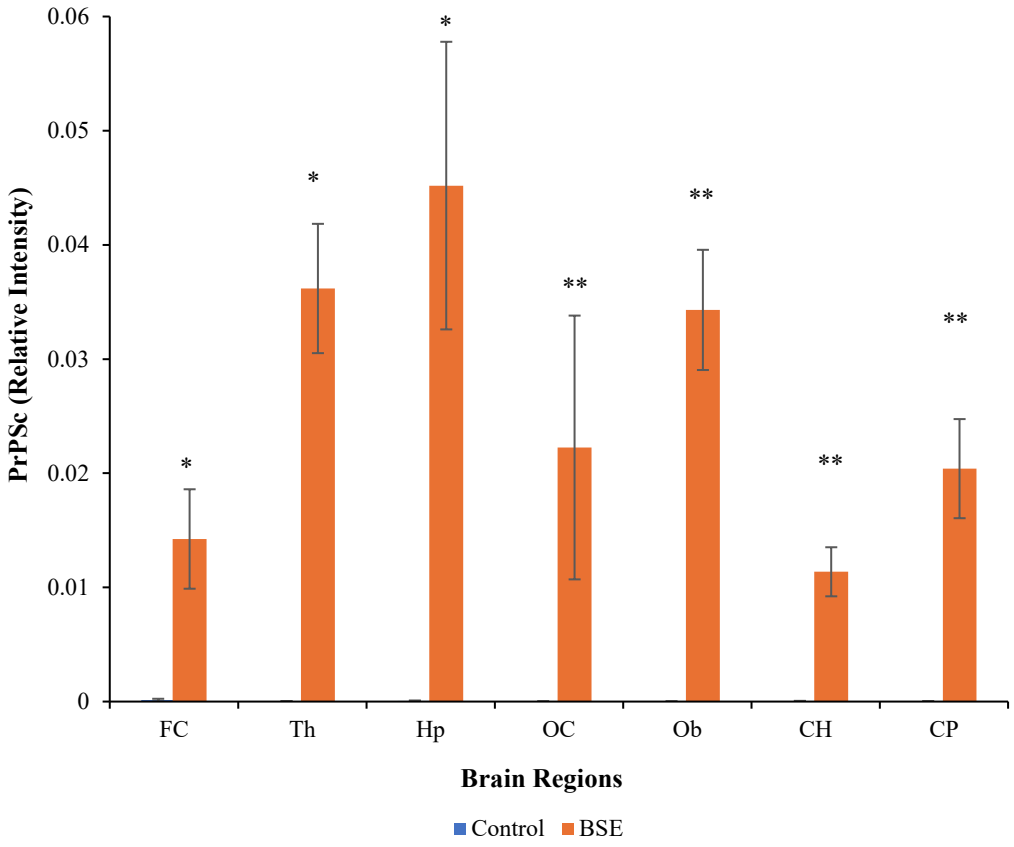

Figure 10: Mean ± SEM of the relative intensity for PrP^{Sc} IHC quantified staining signals across seven regions of the CNS in nine BSE-positive animals combined and three negative controls, with $p<0.05$ (*) and $p<0.01$ (**).

Next, NfL levels are displayed for two groups: negative (n = 3) and positive BSE (n = 9). NfL appeared to be reduced in positive BSE samples; however, this difference was not statistically significant ($p > 0.05$).

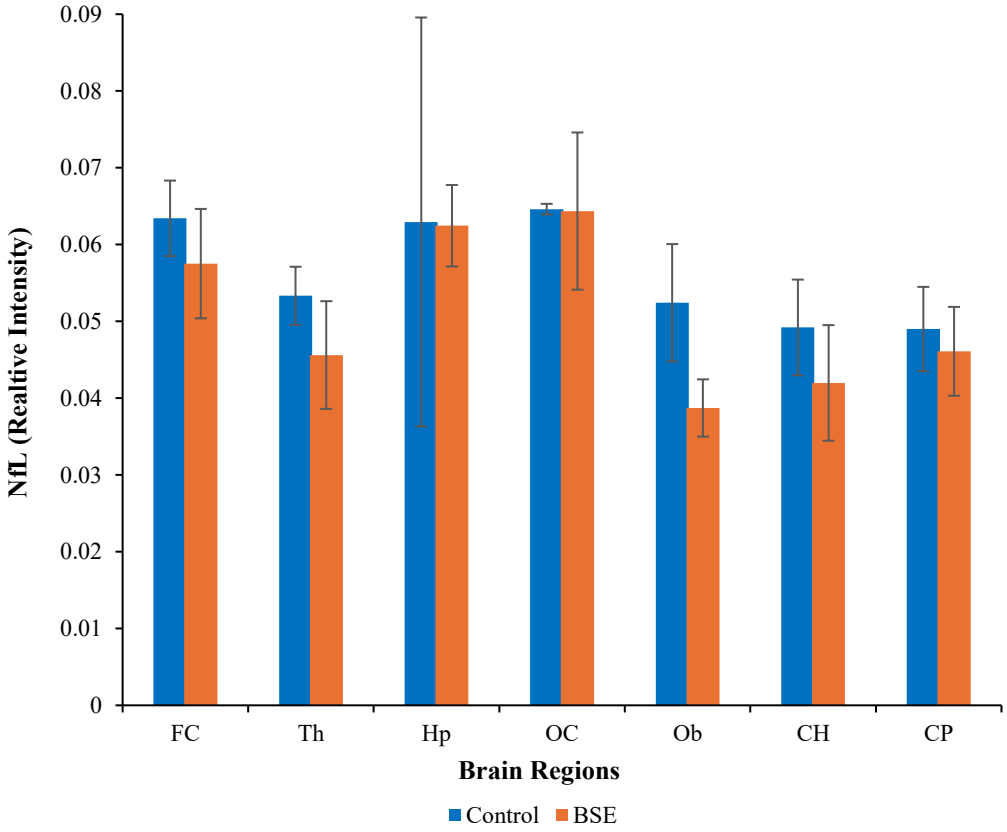

Figure 11: Mean ± SEM of the relative intensity for NfL IHC quantified staining signals across seven brain regions in nine BSE-positive animals, combined with three negative controls, with ($p>0.05$).

When all BSE-strains were grouped as shown in Figures 10 and 11, the Mann-Whitney test showed a significant difference for PrP^{Sc} across all regions. Thus, combining all positive BSE animals into a single group increased statistical significance for the levels of $PrP^{Sc,}$ but not for NfL (Table 5).

Table 5: Mann-Whitney U statistics and exact p-values for PrP^{Sc} and NfL levels, quantified from IHC staining signals in the CNS. Seven brain regions were analyzed in two groups: negative (n=3) and positive BSE animals (n=9).

Brain Regions	**FC**	**Th**	**Hp**	**OC**	**Ob**	**CH**	**CP**
U-Statistics PrP^{Sc}	2	0	0	0	0	0	0
P	0.0364	0.0121	0.0444	0.0091	0.0091	0.0091	0.0091
U-Statistics NfL	12	8	8	12	4	13	12
P	0.8636	0.4970	>0.99	0.8636	0.1	>0.99	0.8636

As with the ELISA analysis, Spearman's correlation was performed on IHC output data, using relative intensities derived from quantified staining signals for both proteins. In Figure 12, the correlation coefficient (ρ) is shown in the individual scatter plots for each of the seven regions, illustrating the line of best fit and indicating the strength of the correlation between the two biomarkers. The frontal cortex exhibited a moderate positive correlation (0.46), which was lower in the cerebellar hemisphere (0.34) and lowest in the hippocampus (0.152), with nearly no correlation at the obex (0.021). A weak negative relationship was observed in the occipital cortex (-0.130) and cerebellar peduncle (-0.207). However, the analysis of the relationship between PrP^{Sc} and NfL intensities across brain regions did not reveal any statistically significant associations.

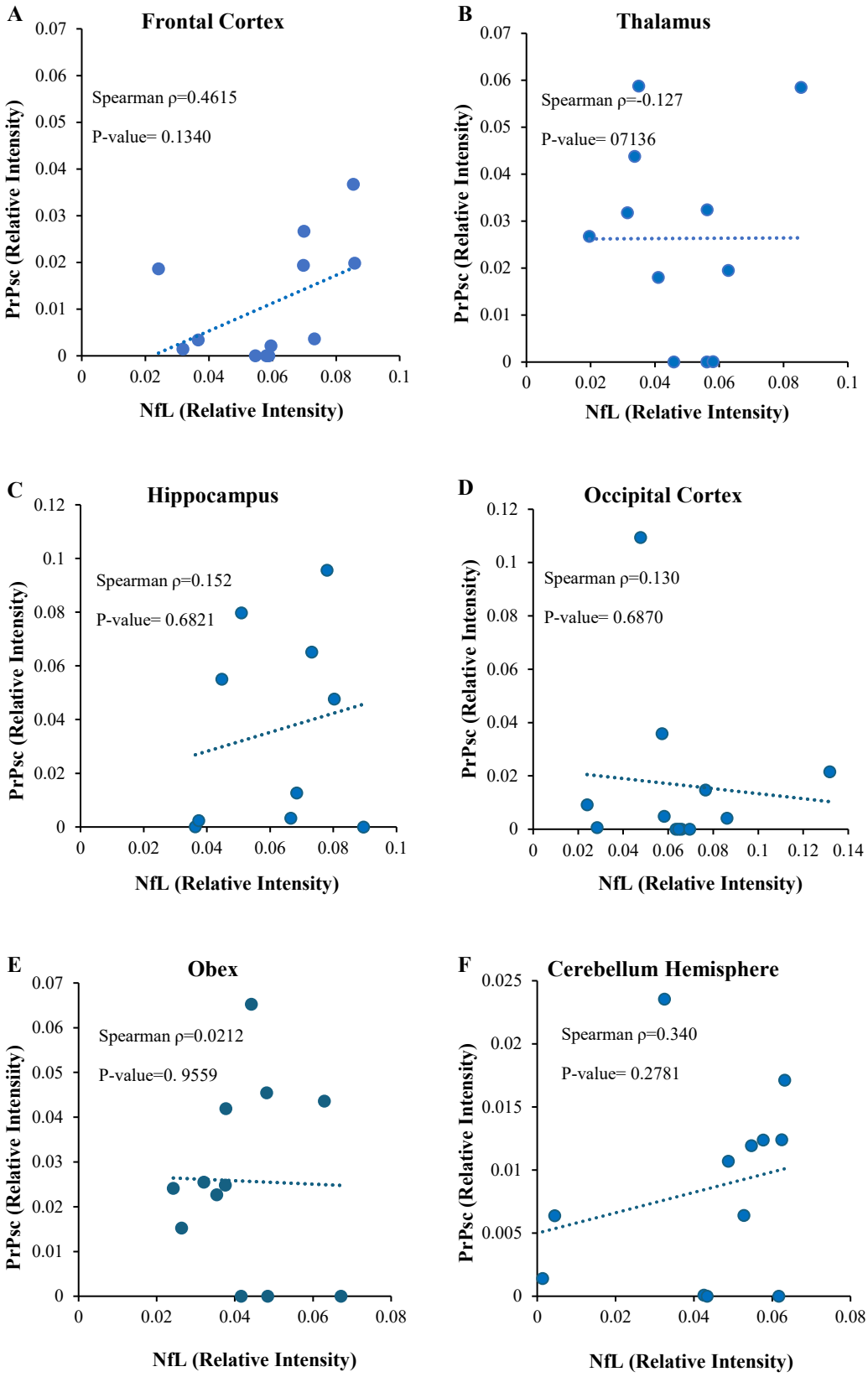
A
Frontal Cortex
Spearman ρ=0.4615
P-value= 0.1340
PrPsc (Relative Intensity)
NfL (Relative Intensity)
B
Thalamus
Spearman ρ=-0.127
P-value= 07136
PrPsc (Relative Intensity)
NfL (Relative Intensity)
C
Hippocampus
Spearman ρ=0.152
P-value= 0.6821
PrPsc (Relative Intensity)
NfL (Relative Intensity)
D
Occipital Cortex
Spearman ρ=0.130
P-value= 0.6870
PrPsc (Relative Intensity)
NfL (Relative Intensity)
E
Obex
Spearman ρ=0.0212
P-value=0. 9559
PrPsc (Relative Intensity)
NfL (Relative Intensity)
F
Cerebellum Hemisphere
Spearman ρ=0.340
P-value= 0.2781
PrPsc (Relative Intensity)
NfL (Relative Intensity)

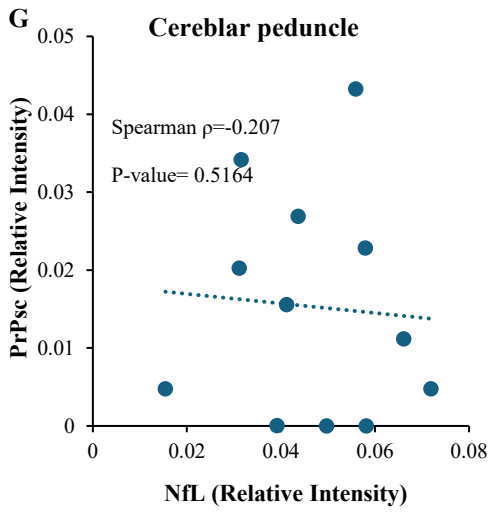

Figure 12: Scatterplot of Spearman correlation coefficients (ρ) between relative intensities of PrP^{Sc} and NfL levels, derived from quantifying IHC immunostaining signals, and their exact p-values. Data are shown for seven brain regions: frontal cortex, thalamus, hippocampus, occipital cortex, obex, cerebellar hemisphere, and cerebral peduncle.

3.2. Evaluation of NfL Levels in Post-mortem CSF of BSE-Challenged Cattle

Thirteen post-mortem CSF samples were tested to analyze NfL levels, as shown in Figure 13. CSF NfL levels were significantly higher in BSE-positive animals than in healthy controls, effectively distinguishing the two groups (Mann-Whitney U statistic = 0, p = 0.0028) (Figure 13A), which is in strong agreement with previous studies [74, 80, 81]. Nonetheless, substantial error bars in the H-BSE and L-BSE groups (n = 2) likely reflect low statistical power, preventing differentiation among BSE subtypes. Despite the large error bars, the negative control remained distinguishable from both C-BSE and H-BSE only (Kruskal-Wallis H-Statistic = 9.079, p=0.005) and in pairwise comparisons (p=0.031 and 0.035) (Figure 13 B). It was essential to assess the effect of age on NfL levels, as previous research indicates that age can also influence NfL release into CSF [28, 63]. The results revealed no effect of age on CSF NfL levels in these BSE cattle (Figure 13C). ROC was

conducted to assess specificity and sensitivity, demonstrating that NfL was both specific and sensitive, accurately distinguishing negative and positive BSE cattle, with an AUC of 1 and p=0.0055 (Figure 13D).

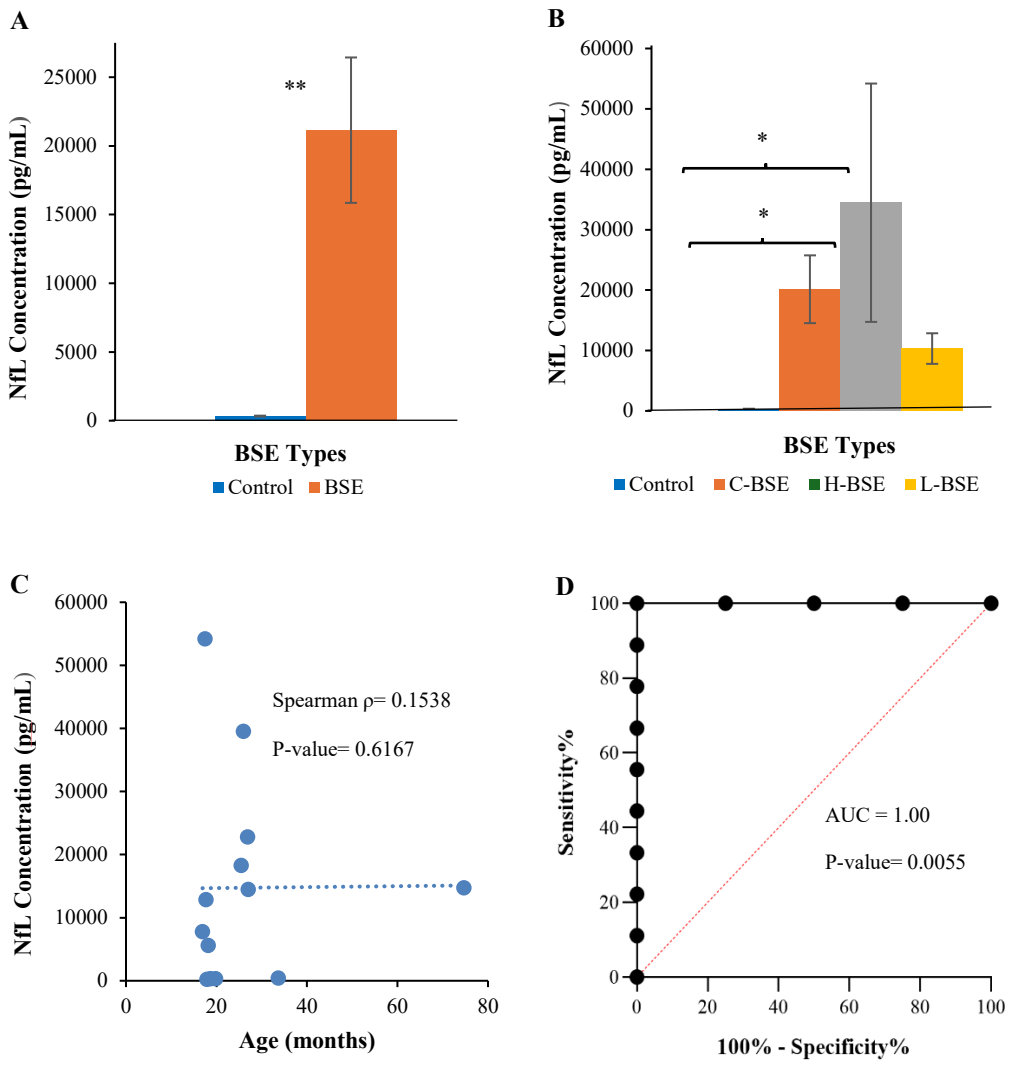

Figure 13: Comprehensive analysis of NfL levels in the CSF of BSE-positive and negative animals. Averaged and dilution-corrected NfL concentrations (pg/mL) (mean ± SEM) were measured using the CSF-NfL kit in two groups (4 controls, 9 BSE-positive), with two technical replicates per sample, and significant differences were detected ($p < 0.01$, **) (A). Comparison of CSF NfL levels between controls and three BSE strains (C-BSE n = 5, H-BSE n = 2, L-BSE n = 2) versus controls (n = 4), showing a significant difference between controls and C- and H-BSE at $p < 0.05$ (*) (B). Scatter plot of CSF NfL concentrations relative to the animals' ages in months, with the Spearman correlation coefficient indicating no significant correlation (C). ROC analysis demonstrates the specificity and sensitivity of NfL levels in CSF (D).

3.3. Evaluation of NfL Levels in Pre-Mortem Blood of BSE-Challenged Cattle

In this part of the study, NfL levels were measured in fifteen pre-mortem serum samples collected from BSE-positive and negative cattle that were alive at the time of blood collection. NfL levels were then compared between the healthy and BSE-infected groups. Data showed that NfL levels were significantly higher in BSE-positive animals than in control animals (Figure 14A), aligning with the CSF results (Figure 13) and other published research [53, 59, 64]. While total serum NfL concentration (pg/mL) distinguished between BSE-positive and negative animals (Mann-Whitney U-statistic = 2, $p = 0.0176$), indicating a notable difference, it did not effectively differentiate among BSE types (Kruskal-Wallis H-statistic = 5.492 and $p = 0.1347$) (Figure 14B). Correlation analysis with age indicated that age did not affect NfL levels in these animals (Figure 14C). ROC analysis showed that NfL was highly sensitive and specific in correctly identifying negative and positive BSE cattle, with a strong AUC of 0.9444 and a p-value of 0.0209 (Figure 14D). Additional samples collected at 75% of the incubation time were also tested to evaluate NfL levels in BSE-positive and negative animals (Figure 14E). The difference in NfL persisted, with higher levels in BSE-positive animals than in negative ones. However, the results were not statistically significant (Mann-Whitney U statistic = 14.5, $p = 0.5375$); although NfL was higher in the positive sample, it remained considerably lower than at terminal stages.

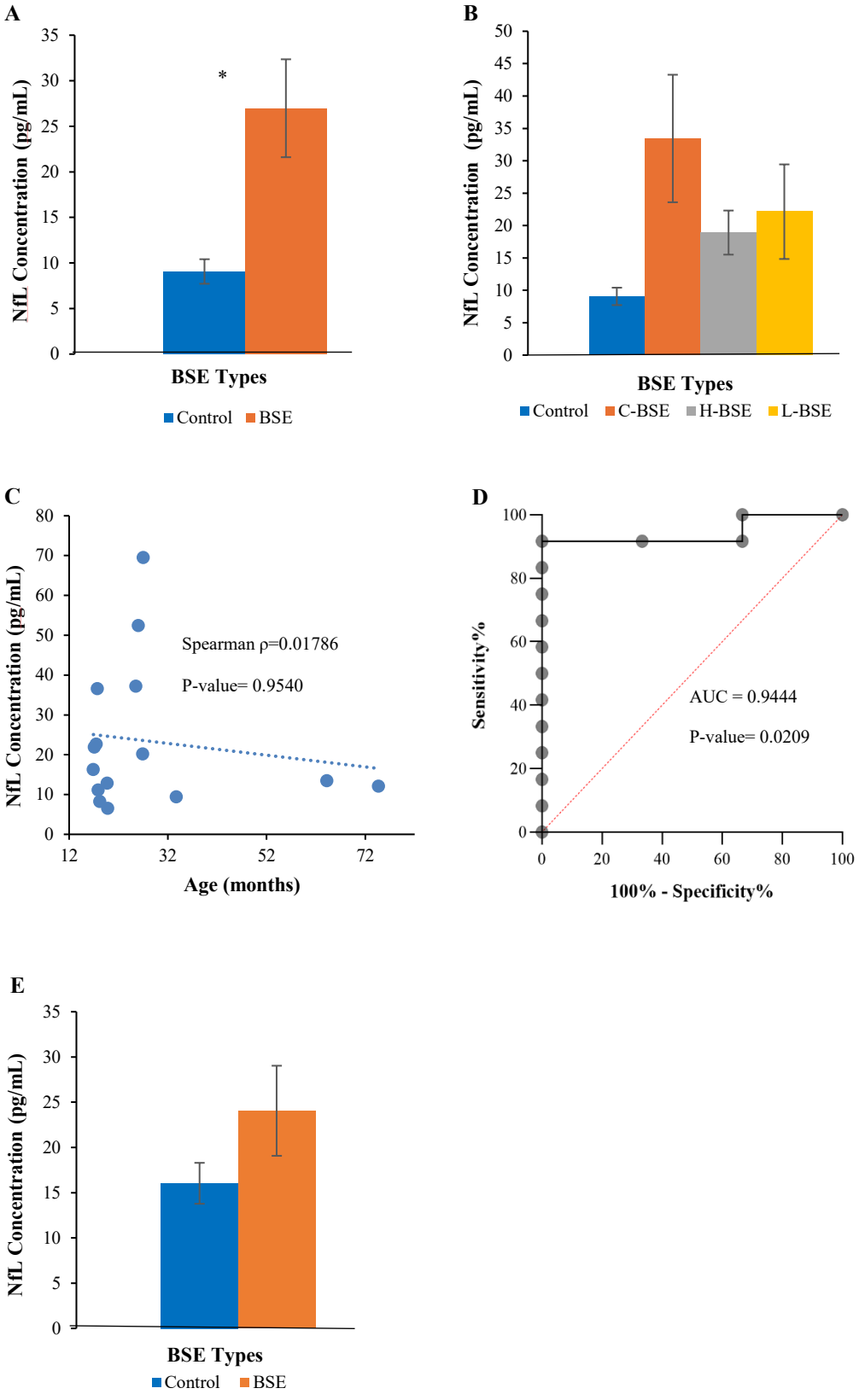
A
NfL Concentration (pg/mL)
35
30
25
20
15
10
5
0
*
BSE Types
Control
BSE
B
NfL Concentration (pg/mL)
50
45
40
35
30
25
20
15
10
5
0
BSE Types
Control
C-BSE
H-BSE
L-BSE
C
NfL Concentration (pg/mL)
80
70
60
50
40
30
20
10
0
Spearman ρ=0.01786
P-value= 0.9540
12
32
52
72
Age (months)
D
Sensitivity%
100
80
60
40
20
0
AUC = 0.9444
P-value= 0.0209
0
20
40
60
80
100
100% - Specificity%
E
NfL Concentration (pg/mL)
35
30
25
20
15
10
5
0
BSE Types
Control
BSE

Figure 14: Comprehensive assessment of NfL levels in clinical premortem serum of BSE-positive and negative animals. Average serum NfL dilution-corrected concentrations (mean ± SEM) were measured using the serum-NfL kit in two groups (3 controls, 12 BSE-positive), with two technical replicates per sample, and significant differences were detected ($p < 0.05$*) (A). A comparison of the average clinical serum NfL concentrations (pg/mL) among the three BSE strains (C-BSE n=6, H-BSE n=3, L-BSE n=3) versus controls (n=3) shows no significant difference among the four groups (B). A scatter plot of serum NfL concentration relative to animals' age in months, with the Spearman correlation coefficient indicating no significant correlation (C). ROC analysis demonstrates the specificity and sensitivity of NfL levels (D). NfL concentrations (pg/mL) measured at 75% of the disease incubation period, with no significant difference between the two groups (p=0.5375) (E).

The analysis summary in Table 6 represents relative statistical data for ROC curves of NfL levels in CSF and serum, shown in Figures 13 and 14. The ROC analysis showed high specificity and sensitivity for NfL in both body fluids, in the presented cohort, with cut-offs that differ between media and clearly show that NfL exist in a lower proportion in blood compared to CSF.

Table 6: Comparison of the ROC analyses conducted for NfL levels in both CSF and serum. The analysis evaluates NfL's accuracy in the two body fluids and assesses its relevance in BSE using 13 CSF and 15 serum samples.

	CSF	**Serum**
AUC	1.00	0.944
Standard Error	0.00	0.0618
P-values	0.0055	0.0209
Specificity	100 %	100 %
sensitivity	100 %	91.7%
Cut off (pg/mL)	>3012	>11.7

Additional correlation analysis was performed between NfL levels in CSF and serum from the same 12 animals (Figure 15). A scatter plot was generated, and a line of best fit was calculated using linear regression to model the relationship between the two variables. The resulting positive slope indicates a positive association, which was further supported by a strong positive Spearman correlation ($\rho = 0.7062$, $p < 0.05$)

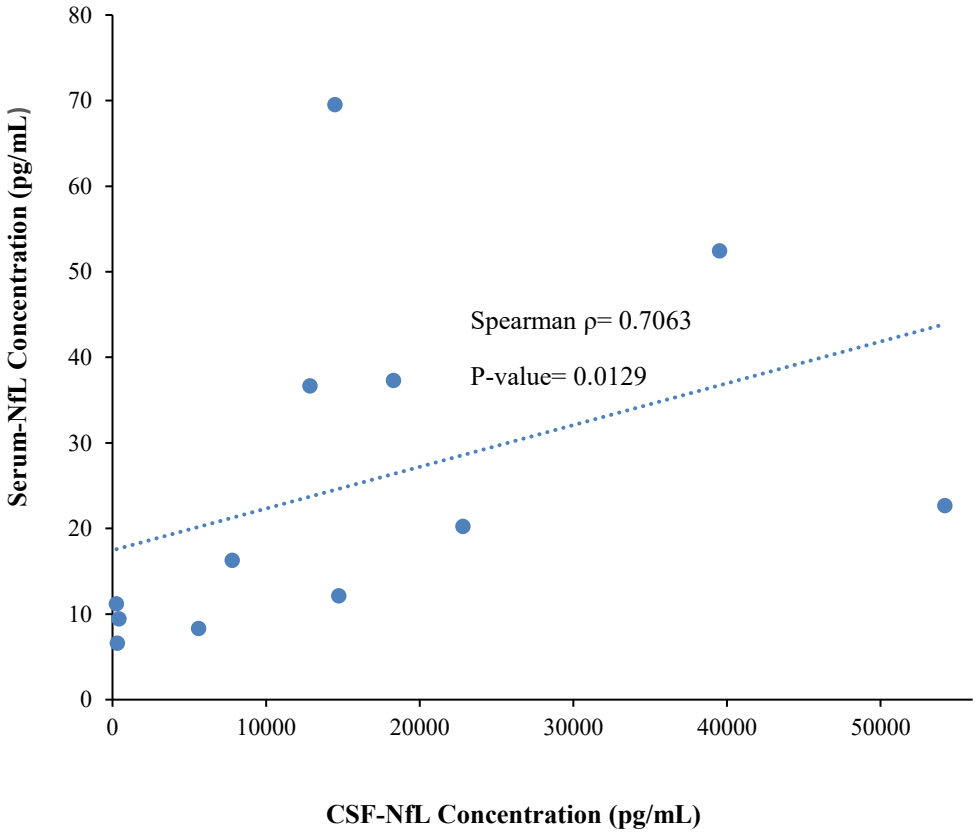

Figure 15: Scatterplot comparing CSF-NfL and clinical serum-NfL levels in the same twelve animals, with Spearman's coefficient (ρ) ($p < 0.05$), indicating a strong relationship between NfL levels in the two biofluids.

3.4. Evaluating the Stability of NfL in CSF and Clinical Blood

Once NfL was established as a successful biomarker for BSE, evaluating its stability was essential to confirm the overall findings. Thus, NfL was evaluated across multiple freeze-thaw cycles and storage temperatures, and the results showed that NfL remained

stable even after numerous freeze-thaw cycles in both CSF (H-statistic 0.6222, p = 0.8286) and serum (H-statistic 0.0889, p = 0.9929) (Figure 16A and B). Additionally, it confirmed the stability of NfL during storage of samples for 5 or 10 days at -80°C, 5°C, and room temperature ~22°C in CSF (H- statistic 1.999, p = 0.7966) and serum (H-statistic 7.208, p = 0.2056) (Figures 16C and D). Therefore, NfL demonstrated strong resistance to degradation, making it a promising candidate as a premortem biomarker for disease detection, including BSE, firmly aligning with previously published data [45].

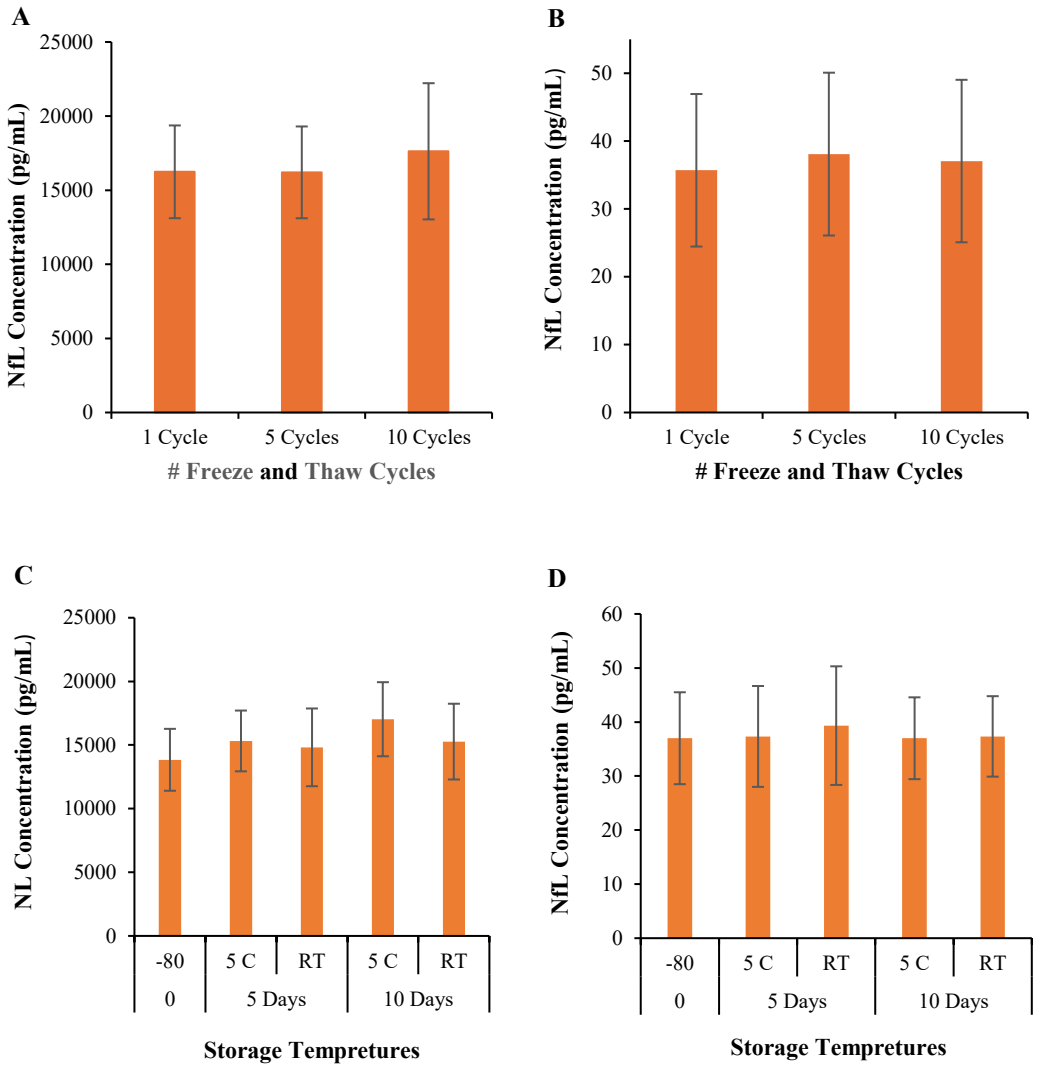

Figure 16: Assessment of NfL stability, where each bar represents NfL concentration in (pg/mL) in three positive C-BSE animals. NfL was evaluated across three freeze-thaw cycles in CSF (A) and clinical serum (B), and at three storage temperatures in CSF (C) and clinical serum (D), with no significant differences observed at any point ($p>0.05$).

4. Discussion

Detecting prion diseases is difficult because the pathogenic agent mainly accumulates in the CNS, and there is currently no validated diagnostic test available to detect PrP^{Sc} in live individuals [64]. This means that the diagnosis of prion diseases is limited only to post-mortem by combining clinical signs, neuropathology, immunohistochemistry for PrP, Western blotting of PK-resistant PrP, as well as PrP types and/ or sequence of *PRNP* gene [65]. Although the development of prion-specific assays in recent years, such as protein misfolded cyclic amplification (PMCA) or real-time quaking-induced conversion (RT-QuIC), has proven effective for premortem diagnosis in humans, these assays are limited to CSF samples [66-71]. On the contrary, collecting CSF samples to diagnose a prion disease in live animals can be invasive and challenging. In such situations, using surrogate biomarkers is a strategy successfully used for diagnosing human prion diseases. Surrogate biomarkers such as 14-3-3 [67, 71, 72], t-tau [67, 71-74], P-tau [67, 71-74], Aβ40-42 [84, [72, 74], total PrP [64, 75] levels in the CSF help diagnose and discriminate from other neurodegenerative diseases, but their sensitivity and specificity vary depending on the prion disease. Additionally, these surrogate biomarkers are limited to CSF samples, making them unsuitable for use in animals. There are other proteins in the CSF, such as neurofilament light chain (NfL) [71, 76], calcium-binding protein S100β [71, 72, 77], neuron-specific enolase [71, 72], α-synuclein and β-synuclein [76-80], neurogranin [76, 77, 79], and SNAP-25 [76, 79], triggering receptor expressed on myeloid cells 2 (TREM2) [74, 77, 81], cytokines [81, 82], and microRNAs [83, 84], shown to be altered during prion diseases, but need further validation. Among these altered proteins, changes in total-tau and NfL could only be detected in the blood and aid in monitoring disease progression in human prion

diseases [60, 85, 86]. Whereas information on changes in total-PrP, synuclein, S100β, TREM2, and peripheral inflammatory markers in blood is limited [65].

Use of such blood-based surrogate biomarkers in livestock, particularly for diagnosing BSE in live cattle, has not yet been explored. BSE in cattle is a zoonotic disease; if undetected, the pathological agent can enter human or animal food and feed chains during slaughter or rendering, and this risk cannot be eliminated. Nonetheless, Canada has strict safeguards to prevent the recycling of the pathological agent by removing specified risk materials (SRMs) during slaughter. Still, the emergence of different prion strains and tissue tropism continues to pose significant risks to public health and livestock. This risk is increased by the possibility when subclinical cattle goes unnoticed. Although the CFIA provides field staff, veterinarians, and farmers with a tool containing information on clinical signs indicative of a potential BSE candidate to help identify animals requiring euthanasia and laboratory testing, misdiagnosis remains possible because clinical signs overlap with those of other livestock diseases. However, many of these animals may test negative, leading to unnecessary economic and emotional stress for farmers. Furthermore, if an animal tests non-negative after euthanasia and during laboratory screening, additional confirmatory tests are conducted to diagnose and classify BSE status. Until these results are available, carcasses may be disposed, rendered or left in the field, posing environmental risks through scavenging. Overall, this emphasizes the importance of pre-mortem screening of clinical BSE suspects to aid in accurate diagnosis at the clinical stage.

To address this knowledge gap, this project aims to explore the pre-mortem diagnostic potential of NfL for BSE. NfL is a well-established and extensively studied biomarker of neuronal damage, relevant to many neurodegenerative diseases, including Alzheimer's [49, 87, 88], Parkinson's [89], brain injury [90], and most specifically prion diseases such as

CJD and scrapie [45, 47]. Under these conditions, brain cells degenerate, and neurons rupture with little to no recovery. NfL is a cytoskeletal protein that supports and protects the structural integrity of neuronal cells and is also released into body fluids such as CSF and blood during neurodegeneration [58, 91]. Studies have shown that NfL levels are higher in the body fluids of individuals with neurodegenerative conditions than in those of healthy controls, with the highest elevation noted in prion diseases, making it a promising biomarker [45]. Since all prion diseases exhibit similar disease pathology, it was expected that NfL would behave similarly, reflecting neuronal damage in BSE, as was the case in prion diseases in other species such as scrapie and CJD [45, 58, 92].

Before exploring NfL's potential as a premortem disease indicator, it was essential to investigate its relevance in cases of BSE and examine its correlation with the deposition of the pathogenic agent. Other studies have shown a negative correlation between the two proteins, with NfL decreasing in brain regions with high PrP^{Sc} abundance [58]. They suggested that higher PrP^{Sc} levels in the brain lead to severe neuronal damage, resulting in the rupture of neurons and the release of disrupted NfL from the brain into body fluids including CSF and blood. This would lead to reduced NfL levels in the brain but elevated levels in the CSF and blood of positive cases. To track the phenomenon of NfL clearance from the brain into body fluids due to neuronal damage, both NfL and PrP^{Sc} levels were measured using ELISA and IHC in various regions of the brain of negative and positive BSE-infected cattle. The association between the two markers was evaluated using Spearman's correlation analysis.

IDEXX EIA results showed that PrP^{Sc} was absent in control animals but clearly present throughout the brain in positive BSE cases (Figures 1 and 3). The distribution pattern of PrP^{Sc} varied among BSE strains and across brain regions. Although all tested animals were

experimentally challenged under controlled laboratory conditions, uniform deposition was not observed, confirming that PrP^{Sc} exhibits strain-specific selectivity, as previously reported [37, 93]. The results of the current investigation showed that prion strains exhibit distinct patterns of PrP^{Sc} distribution, with significant differences which may be also due to the so-called P2 animals. Those animals were intracranially inoculated; however, the inocula (brain homogenates) were derived from orally challenged animals, whereas the remaining animals were inoculated with brain material from intracranially inoculated animals. Initially, those animals were assumed to be negative because of their extremely long incubation periods compared to others. Still, they were later confirmed to be positive, with a low prion prevalence. This resulted in a unique pattern that deviated from the rest of the data, which might have led to the current apparent large error bars and variability.

NfL levels measured by ELISA showed larger error bars than those seen for PrP^{Sc} analysis, and their pattern also differed (Figures 2 and 4). The pattern did not follow a clear trend but rather appeared to be a randomly distribution, comparable between negative and positive cases. However, when examining NfL, it is crucial to consider all potentially relevant factors that could influence the results, beyond the inclusion of P2 animals. These factors include the nature of NfL structures, which consist of distinct domains, including head, rod, and tail [49]. These domains may also exist as fragments depending on the biological medium (brain tissue or bodily fluids), as well as the type of neurodegenerative condition and associated proteolytic activity [49, 94, 95].

NfL primarily exists as a full-length in the brain, with a small proportion of C-terminal truncations, whereas only short fragments are detected in the CSF [49]. However, the human-derived Quanterix kits are designed to detect NfL fragments solely in CSF, potentially failing to bind to full-length NfL species present in the brain and limiting the

ability to differentiate healthy from infected cattle. This issue became more evident during NfL measurements in brain tissues, as nearly all samples fell outside the kit's detection range of 125-2500 pg/mL. As a result, all samples required multiple tests at dilutions ranging from 3000- to 9000-fold, with dilution factors optimized individually for each sample to bring concentrations within the kit's detection limits, underscoring some of these kits' limitations. While this approach allowed for quantification, it may have led to additional variability in the data, with dilutions inconsistent across samples, which might also have affected the overall picture of NfL.

Correlation analysis was conducted on the overall ELISA results to compare the levels of both proteins and examine any potential relationship between PrP^{Sc} and NfL. The Spearman coefficients varied in magnitude and direction, and none were statistically significant. This inconsistency suggested that there was no clear association between the two markers based solely on ELISA results. Several limitations were identified, including the small sample size (n = 3 per group, or n = 2 in some cases), variability in sample preparation, variation in BH amounts (~0.30 ± 0.05 g), the use of P2 animals, and reliance on human CSF kits due to the lack of brain-specific assays. As a result, the correlation analysis may not accurately reflect the true association between the two proteins.

Therefore, knowing that NfL exists mainly as fragments in CSF, which originally come from the brain, where they are initially present as full-length proteins, it is assumed that only selective fragments leave the brain and enter the CSF. The full-length NfL is composed of multiple domains containing coil 1A, coil 1B, coil 2A, and coil 2B, which are all connected and stable in intact NfL [49]. Hence, NfL found in CSF would represent a smaller fraction of those present in the brain at any point during neuronal damage, where their structures would be altered by fragmentation, thereby affecting their bindings to

antibodies and making them different from those in the brain. Thus, testing NfL species in the brain using those CSF kits led to unequal detection of all proteins, as antibodies are designed to bind to specific epitopes that could be masked when NfL is present in its full-length. Most ELISA kits are designed to capture particular NfL fragments, either in CSF or in blood, and to recognize the epitope region containing coil 2B in most cases [49, 57]. Thus, it might be hard to access those proteins in the brain, as their binding wouldn't be optimal. This is why there are different kits designed for each body fluid, given the distinct proteolytic processes that give each its final structure, as NfL fragments differ and have been identified in CSF [68] and blood [57, 94, 96]. These structural variations are also supported by previous literature, which shows that alterations in NfL can lead to structural disturbances, functional impairment, and cross-linking and tangle formation, thereby altering the actual structure and most likely affecting interaction with antibodies [97].

Additionally, analyzing NfL levels in the brain using the CSF NfL kit presents a much more complex challenge than assessing NfL in CSF. Brain tissues are heterogeneous, highly structured organs that contain various cell types, including neurons, glial cells, and endothelial cells, each of which may contribute differently to NfL release, as NfL exists in different abundance throughout the brain [98, 99]. This complexity may affect assay performance, making it more challenging to obtain uniform, consistent measurements of NfL levels across different brain regions. Given these limitations, it was essential to perform this analysis using a more reliable approach, such as immunohistochemistry (IHC), a well-established confirmatory technique in prion research.

Hence, staining the brains of BSE positive animals for PrP^{Sc} with anti-PrP antibody F99 and quantifying PrP^{Sc} immunolabelling (as shown in Figures 7 and 10), showed overall levels of PrP^{Sc} in agreement with those from IDEXX EIA. No PrP^{Sc} signal was observed

in the negative controls, while positive samples showed apparent immunolabelling throughout the brain. However, when the four BSE groups were plotted separately, no significant differences were observed; in contrast, combining all BSE stains revealed more pronounced differences, highlighting the impact of sample size on the reliability of the outcomes (Figure 10). These differences may stem from limitations such as sample size, experimental procedures, and the availability of tissue blocks for staining.

Similarly, the quantification of total NfL levels after staining BSE-positive brains with ant- NfL antibody (as shown in Figures 9 and 11), indicated a pattern in which, in most cases, NfL is lower in BSE-positive animals than in controls, except for a few C-BSE cases, none of which were statistically significant (Figure 9). Upon combining all BSE strains, the pattern becomes clearer, and NfL seems to be reduced in BSE-positive samples compared to controls (Figure 11), aligning with previously published results [58]. This decline in NfL is likely due to ongoing neuronal damage at any given time, which may be released into body fluids [28, 50, 100]. Such processes can occur through homeostatic mechanisms that the brain uses to manage neuronal damage when axons are ruptured, releasing damaged NfL [48, 96]. The exact clearing mechanism is not fully known, but it is speculated to involve many different pathways, including the activation of microglia cells for clearance [28, 101], internal degradation inside neurons (proteasomes, autophagy) [102], or by releasing it to the extracellular space, where enzymes outside the cell break it down [103]. This underscores the dynamic nature of NfL across the brain, accounting for regional variation in its concentration [98, 99]. Consequently, levels may rise in one area and fall in another, reflecting the current state of neurodegeneration and clearance.

In the present investigation, Spearman correlation analysis was performed similarly to ELISA, and the correlation coefficients varied across brain regions, with some areas

showing no or low correlation (obex) and others showing moderate positive correlation (frontal cortex). However, none of these correlations reached statistical significance, suggesting that the observed associations may be weak or confounded by variability in the data presented compared with those reported in previous studies [53], which showed a strong negative correlation [58]. The Spearman coefficient was low in the obex regions, indicating that the levels of both proteins are independent. This could be because the PrP^{Sc} is typically present in the brainstem early in the disease, and where most damage is expected to occur. Thus, it is anticipated that NfL in this region would have reached its optimal level by the time the disease reaches the terminal stage, when disrupted NfL is cleared into the CSF to maintain homeostasis during disease progression [28, 104]. Given that this area is rich in myelin, where most of the NfL would be present [48], this suggests that NfL levels may have been higher at earlier stages of the disease, as shown in an early study, where NfL was found to be higher at preclinical stages of scrapie [58]. This could explain the apparent lack of connection between the two proteins in this area. Eventually, in the final stages of the disease, it is hypothesized that the pathogenic agent would reach the frontal lobe, particularly in the later stages, when ρ is higher, possibly exhibiting the least neuronal damage; hence, both NfL and PrP^{Sc} are elevated simultaneously. Thus, NfL would remain intact and less regulated, as PrP^{Sc} has not caused severe damage in this area. Therefore, in cases where NfL levels are unchanged or similar between negative and positive BSE (Figure 11), this may indicate minimal disease manifestation and a possible early clinical stage. Conversely, reduced levels might be observed at the terminal stages of the disease, with greater damage.

Therefore, it is crucial to consider the differences between this and the other study, which examined NfL using IHC. Betancor, M., et al., had focused on various stages of the

disease, analyzing the negative, pre-clinical, and clinical stages in sheep [58]. This allowed researchers to accurately determine the disease stage in each animal, whereas the animals used here were euthanized once clinical symptoms appeared. However, as shown in Table 1, their ages varied, indicating they might not all be in the same clinical phase, with some possibly being in early or mid clinical, or terminal phase. While a negative association between NfL and PrP^{Sc} was observed in scrapie (21 animals), no such association was observed here (12 animals), with three of the latter being P2 and showing trends different from the rest of the cohort. Thus, it is suggested that multiple factors could explain the observed lack of correlation between NfL and PrP^{Sc}, and that NfL might not necessarily correlate with PrP^{Sc} deposition but rather with the neuronal damage it causes, as has been well established in other studies [63]. Still, visual inspection of the bar graph suggests lower NfL levels in positive samples, indicating a possible negative correlation; however, no statistically significant difference was observed. This may be attributed to the previously mentioned limitations, which could mask any true association despite the observed trend

The overall output of NfL analysis can be influenced by various factors that affect interpretation, including variability in incubation times among animals, as shown in Table 1. In the P2 animals, those with the most extended survival had low levels of PrP^{Sc}, which is why they were initially thought to be negative. However, it has been suggested that neuronal damage in these animals was less severe than in other positive animals. Therefore, the pattern of NfL may vary depending on neuroanatomical factors; in this case, the prions were present in limited amounts and did not cause severe damage, having an altered trend in these animals compared to the rest. This regional variability could lead to significant differences in NfL levels, complicating the establishment of a consistent relationship between NfL levels and prion deposition across all regions. The assessment of NfL levels

in the brain is complex and likely involves additional underlying dynamics that are not yet fully understood. This was demonstrated in the study of by Betancor, M., et al., 2022, although a negative correlation was observed in the brain and explicitly suggested downregulation of NfL, the NfL gene was highly expressed in some brain regions of positive animals compared to controls [58].

Additionally, technical factors such as antibody selection [57], as well as complex brain pathology from non-prion causes, can influence NfL levels [28, 104]. Therefore, this type of research would benefit from additional controls to develop a more comprehensive understanding and to provide clear answers regarding the significance of NfL in brain pathology. These controls should include strict adherence to the inoculation procedure, achieved by limiting the task to a single person, using inoculum from the same source, and maintaining a consistent incubation period, which is particularly challenging and unpredictable. In practice, many of these control measures are difficult to enforce, especially with large animals that require prolonged monitoring and intensive care, making strict control over incubation and preservation impractical. Future studies should examine these strains separately to understand their distinct effects on pathology and biomarker levels, using a larger cohort to increase statistical power.

Overall, NfL is constantly changing and challenging to track throughout disease incubation time. Thus, it appears that NfL might also indicate the rate of pathological progression or disease aggressiveness, as previously determined [105]. It has already been established that NfL is primarily influenced by neuronal damage and advancement over time; therefore, it is time-dependent throughout the course of the condition [66]. However, this was also expected, given ongoing damage in the positive sample, which led to axonal disruption, NfL fragmentation, and increased brain leakage due to disruption of the blood-

brain barrier [100]. Due to the previously mentioned limitations of ELISA, IHC appears to provide a more reliable answer.

Following the brain correlation analysis, NfL levels in body fluids were assessed to further validate the observed pattern, which was achieved by measuring NfL levels in CSF, particularly to evaluate their relationship to brain levels and to other prion strains. This step was imperative, as prior research demonstrated that NfL levels were higher in prion disease positive CSF samples than in controls, reflecting the neuronal damage [104, 106, 107]. Therefore, the link between NfL levels in the brain and CSF was previously hypothesized to reflect the quantity released by dying neurons [100].

Upon testing CSF samples with the Quanterix CSF-NfL assay, NfL levels were significantly higher in BSE-positive cases ($p = 0.0028$) compared to controls (Figure 13). When comparing BSE types, NfL levels were elevated across all three BSE strains (Figure 13A and B). Among the positive samples, H-BSE showed the highest NfL concentration, followed by C-BSE and L-BSE (Figure 13 B). However, the large variability (as reflected by the error bars) resulted in differences that were not statistically significant, preventing NfL from distinguishing among the three BSE types. Significant differences were observed between the control and C-BSE and H-BSE ($p = 0.031$ and $p = 0.034$), confirming NfL as a marker of neuronal injury as previously reported [48, 63]. These findings support earlier research indicating that this increase results from neuronal impairments caused by prions, leading to the release of NfL from the brain into CSF [63, 78]. These results demonstrate the benefits of using NfL as a biomarker, as it increases following neuronal injury [48]. The process by which NfL enters body fluids is not fully understood. However, it may involve the glymphatic system, as its function could be impaired, leading to reduced clearance control and allowing large molecules, including NfL species, to enter surrounding fluids

[70, 71, 74, 75]. Total CSF NfL reflects contributions from different brain regions and indicates the amount released from the brain [78]. The current BSE study also showed variation in NfL levels across different brain regions, which likely contributes to the total NfL measured in CSF and aligns with observations in various human diseases [37].

However, the results of NfL analysis using human CFS kits highlighting species-specific differences in NfL levels and emphasizing the need for bovine-specific diagnostic tools [92]. This may indicate greater neuronal degeneration in BSE, but it needs comparative analysis with human CJD CSF samples. This suggests that differential diagnosis with other neurodegenerative diseases in livestock could be made if cut-offs are determined after developing a bovine-specific kit. Although NfL appeared successful at separating healthy cattle from infected ones, it did not distinguish between BSE subtypes, with only two samples per subtype (H and L-BSE).

The low number of atypical BSE samples was a significant limitation in this study. This is mainly due to the fact that only around 100 atypical cases have been reported worldwide, compared to thousands of classical BSE cases. As a result, the availability of materials for experimental studies is very limited, which restricted both the number of samples that could be included and the ability to generate additional research samples in the lab. This made it difficult to fully understand the impact of atypical BSE cases on overall NfL levels, as well as how the limited number of samples may have influenced the results. Further investigation of NfL across the three strains would be important to determine whether patterns differ, how these findings compare to prion diseases in other species, and whether the overall outcomes align with published research.

ROC analysis shows high specificity and sensitivity when using CSF NfL levels to distinguish infected cattle from controls (AUC=1, $p=0.005$), with a cut-off >3012 pg/mL

and no variability in the data (Figure 13 D). This indicates that CSF NfL is highly suitable for ELISA testing in BSE cattle, achieving 100% specificity and sensitivity. Essentially, CSF is reliable for identifying all negative and positive BSE cases accurately. Furthermore, the Spearman correlation analysis of CSF NfL levels and age showed no relationship, ruling out the possibility that CSF-NfL levels are age-dependent, at least in this study (Figure 13C).

Although evaluating NfL in CSF was successful, CSF collection is invasive for animals, so it is preferable to find a method that can be used in accordance with the animal's health status. Additionally, this was crucial to understand that all prions share a common pathology, by demonstrating that NfL would reach the blood in these BSE positive animals, similar to what is shown in both scrapie infected sheep and CJD affected humans, and determining the relative amount present in blood compared to CSF. Therefore, the goal of this project was to evaluate NfL levels in blood as a premortem diagnostic for BSE, which would be less invasive than lumbar puncture because it would require only a blood sample. Results from serum analysis showed that NfL was higher in positive BSE samples compared to healthy cattle but many orders of magnitude lower than those found in CSF, effectively distinguishing between the two groups of animals. Thus, it provides a premortem method for BSE detection and overcoming the limitations of post-mortem screening (Figure 14A), which strongly aligns with previous studies in humans and sheep [22, 45, 56, 91]. However, the study unfortunately did not differentiate among the three BSE types (Figure 14 B), likely due to the small sample size.

While the animals' ages were initially a concern because of the variable incubation periods, which also varied by strain, the age factor was dismissed as a possible influencer on elevated NfL levels in blood. This was confirmed by the lack of correlation (Figure 14C)

and this clearly demonstrated that total NfL levels were independent of age, as the correlation was low and not statistically significant, in contrast to other studies indicating that NfL increases with normal ageing [63].

Furthermore, ROC curve analysis indicated that NfL testing in blood exhibited very high specificity and sensitivity, at least in this study, yielding (AUC=0.94, p=0.0209) with a cut-off of >11.7 pg/mL, and greater variability among data points (Figure 14D). It achieved 100% accuracy in identifying all control cases and 91.7% sensitivity. Despite high specificity, serum NfL was less effective than CSF; however, given the small cohort in this study and the 91.7% test sensitivity, this is notable.

Additional testing of NfL levels at 75% of the incubation period provided valuable insights: as NfL was higher in the positive BSE group compared to healthy controls at that timepoint; however, the difference was not statistically significant (Figure 14E). It is important to note that this stage occurred many months before the appearance of clinical signs. This indicates that NfL has strong potential to differentiate between BSE-positive and negative animals at or just before the clinical stage. Furthermore, the highest levels were observed during the clinical phases, reflecting the most severe neuronal damage as the disease progresses. Therefore, NfL release from the brain into CSF and then into the bloodstream tends to increase as neuronal damage peaks. Consequently, testing NfL during the clinical stages offers the best chance for successful BSE detection [74]. This supports NfL as a promising premortem clinical biomarker for BSE, particularly when combined with specific clinical signs.

Given the observed similar pattern of NfL across both body fluids, with elevated NfL levels in BSE-positive cases compared to healthy controls, an association between NfL levels was expected. As a result, Spearman's rank correlation was used to assess the strength

of such a relationship. A strong positive correlation of 0.7 was identified, which is not perfect but sufficiently high to suggest that NfL levels in both body fluids tend to increase together. This implies that animals with high CSF NfL levels are likely to have elevated blood NfL levels and to show a greater increase in blood NfL levels when neuronal damage is more extensive. The scatterplot shows that NfL levels increased proportionally in both CSF and serum, consistent with previous studies reporting a positive correlation [61].

When evaluating a protein's potential as a biomarker, understanding its stability is essential, as proteins are often sensitive and prone to instability. In this context, obtaining accurate results unaffected by factors such as freeze-thaw cycles and storage temperatures was vital, as these can significantly impact sample quality and diagnostic test results. Our results show that NfL remains stable through freeze-thaw cycles when samples are reused and across different storage temperatures, during long-term storage, aligning well with earlier research [59]. Data on the NfL stability assessment indicated that NfL is less susceptible to degradation than many other proteins, thereby helping preserve samples and enabling repeated testing. Thus, NfL appears to be a practical biomarker because it is easy to handle and requires fewer control measurements.

Therefore, the success of NfL as a potential premortem biomarker would help reduce the cost of diagnosing BSE, as all BSE clinical-suspect cattle are currently euthanized for screening, which adds a financial burden. It also provides a quick screening tool that saves time by using blood for NfL testing. Results from blood NfL testing can be obtained within a few hours, compared with current approaches, which are limited to slower post-mortem tests that require animal sedation, transport to an appropriate high-contamination-level lab for autopsy, and additional challenges in handling large animals. The post-mortem process also requires a veterinarian and significant team effort to complete, as well as the collection

of samples under a pathologist's supervision for accurate identification of brain tissues. Then, tissue collection, which followed screening (usually a one-day ELISA test), with results coming back negative most of the time. Thus, NfL provides a practical, time-effective tool that would improve the cattle industry by enabling quick, premortem screening before proceeding to post-mortem for ELISA, thereby providing an additional confirmatory step early on before the initial screening. Consequently, NfL seems to be a key area of interest that, if confirmed as a reliable biomarker, could advance prion research and inspire further investigations.

5. Future Directions

NfL was able to successfully distinguish between healthy controls and BSE-positive animals in premortem blood samples with high specificity and sensitivity. While this is a strong finding, extending this analysis to evaluate NfL specificity and sensitivity in other cattle-related neurodegenerative diseases could provide further insight. This would help clarify how similar those conditions are to BSE when evaluating NfL and how far they are from humans, where NfL is well explored and found to be a marker of many diseases, with elevation being most significant in prion diseases. Therefore, it is also essential to differentiate BSE from other neurological disorders, as many of them share similar clinical symptoms and might be mistaken for BSE. These diseases include listeria, lead poisoning, and polioencephalomalacia, which are split into thiamine deficiency and sulphate toxicity, vitamin A deficiency, pituitary abscess, ketosis, hypomagnesemia, and middle ear disorders [108]. Since NfL is a general marker of neuronal damage, its elevation is not specific to BSE and has been reported across a range of neurodegenerative conditions. For example, increased NfL levels have been well documented in human prion diseases such

as Creutzfeldt-Jakob disease [45, 46, 85], as well as in other neurological disorders, including Alzheimer's disease [87, 88] and multiple sclerosis [28, 105]. This highlights the importance of assessing whether NfL can reliably distinguish BSE from other neurological conditions in cattle. It remains unclear whether differences exist in the magnitude or pattern of NfL elevation between diseases, whether species-specific variations influence NfL levels, and whether a diagnostic threshold can be established to accurately differentiate BSE. Addressing these points would improve the interpretation of NfL as a biomarker and help determine its true diagnostic specificity

If future studies are successful and NfL proves to be a promising tool that accurately differentiates between all bovine neurological disorders, or at least indicates neuronal damage, this could help improve the industry by removing diseased cattle from herds. So, the success of NfL can improve the quality of livestock imports and exports, thereby reducing the costs associated with their inclusion, which arise from the lack of reliable identification methods.

Supplementary Section:

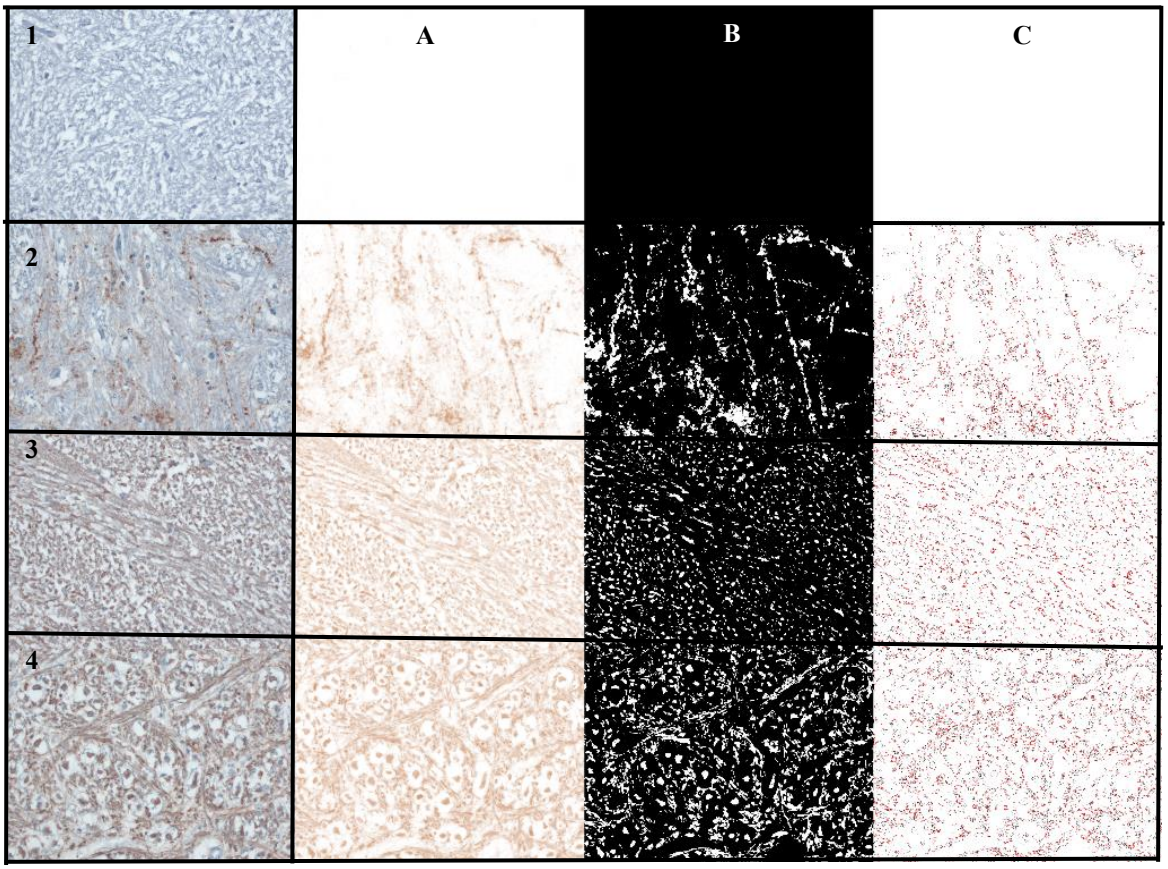

Supplementary Figure 1: Digital quantification of IHC staining signals for PrP^{Sc} and NfL levels using Image J software. The process applies colour deconvolution to separate the brown DAB staining (A), then uses binary and watershed techniques to distinguish fused cells (B), followed by analysis and measurement of the intensity of selected cells (D) in the obex region stained for PrP^{Sc} in a negative control animal with ID 27031 (A) and a positive C-BSE animal with ID 29024 (B). The same animals are stained for NfL, including a negative control (3) and a C-BSE (4) animal.

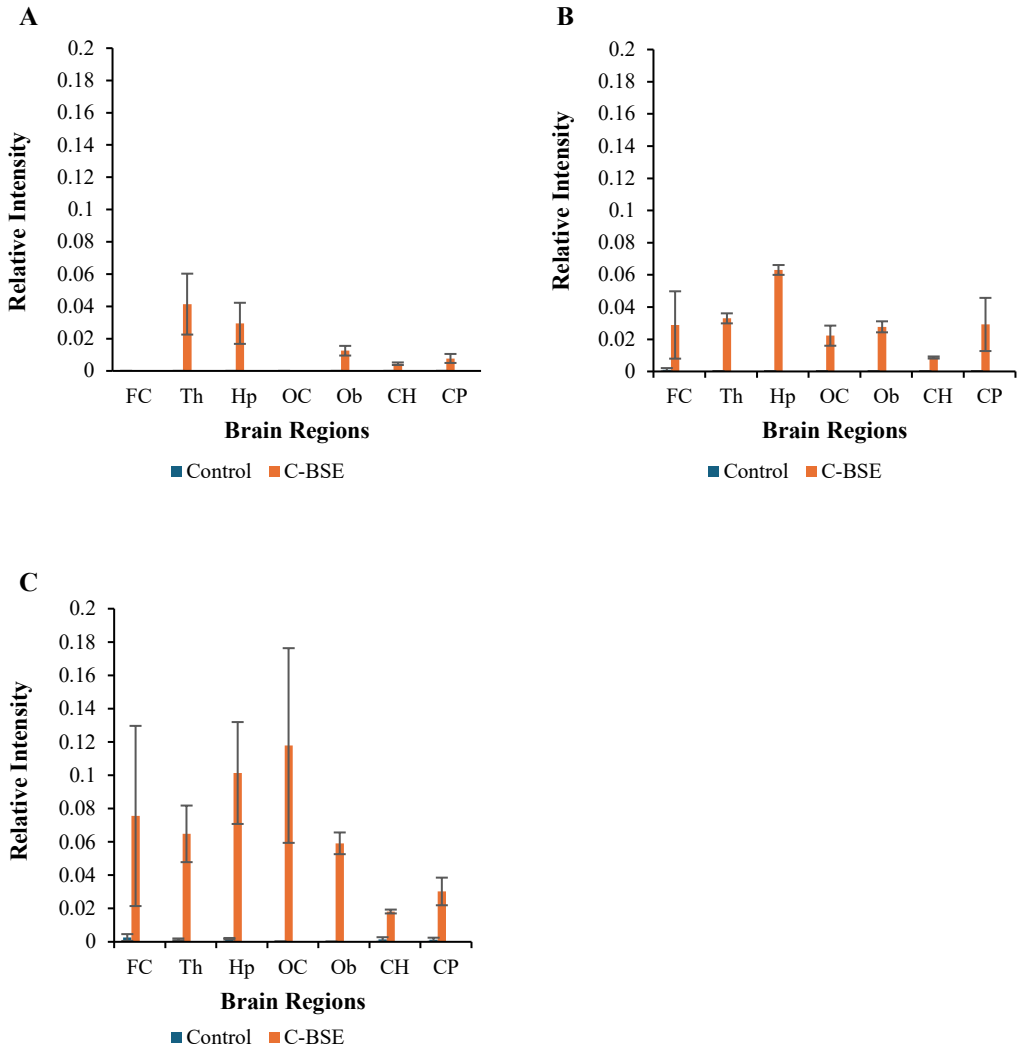

Supplementary Figure 2: Optimization for quantifying IHC anti-PrP staining signals in three healthy controls and three C-BSE samples across seven brain regions, including the frontal cortex (FC), the thalamus (Th), the hippocampus (Hp), the occipital cortex (OC), the obex (Ob), the cerebellar hemisphere (CH), and the cerebral peduncle (CP). Quantification tested three thresholds to measure relative intensities, displayed as bars: 0-175 (A), 0-200 (B), and 0-217 (C), to accurately identify valid signals and exclude background and non-specific staining.

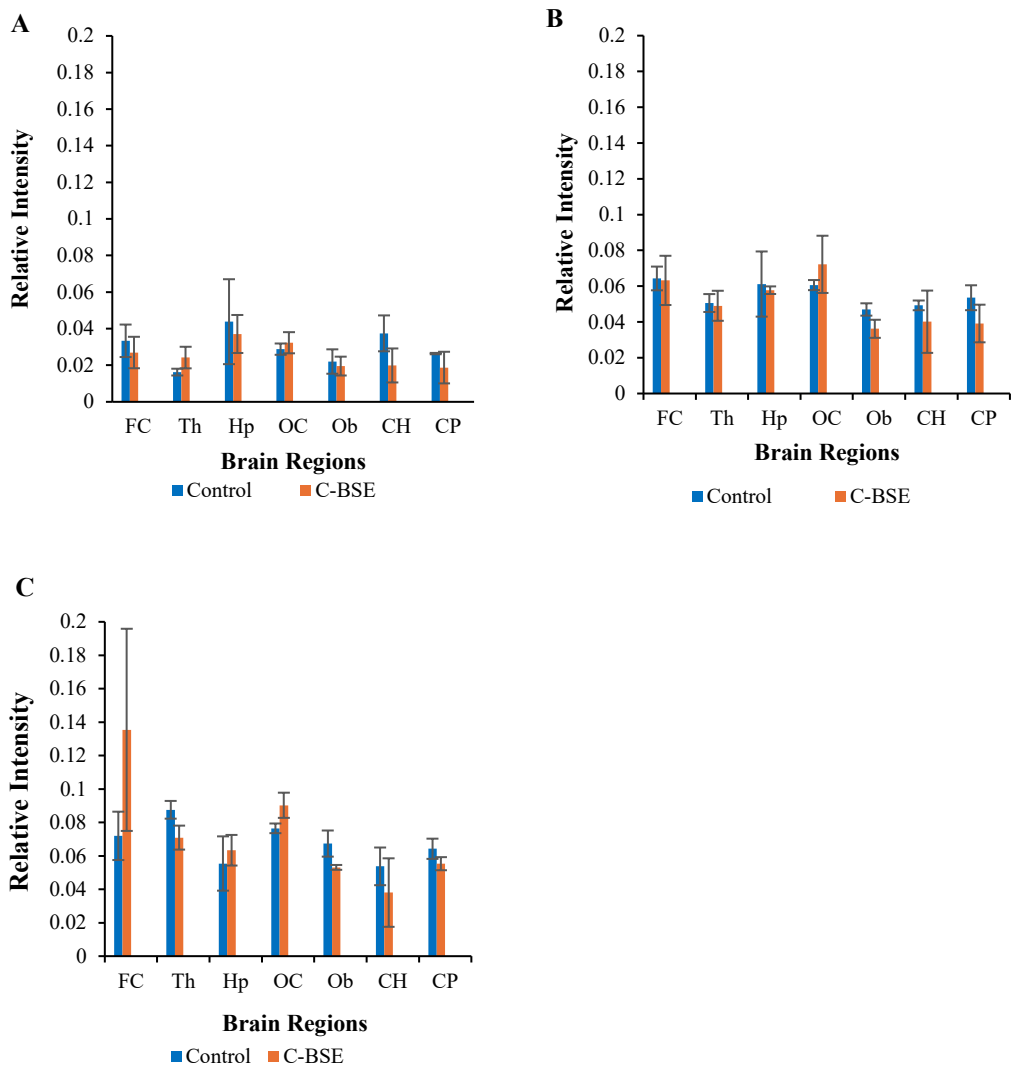

Supplementary Figure 3: Optimization for quantifying IHC anti-NfL staining signals in three healthy controls and three C-BSE samples across seven brain regions, including the frontal cortex (FC), the thalamus (Th), the hippocampus (Hp), the occipital cortex (OC), the obex (Ob), the cerebellar hemisphere (CH), and the cerebral peduncle (CP). Quantification tested three thresholds to measure relative intensities, displayed as bars: 0-150 (A), 0-175 (B), and 0-200 (C), to accurately identify valid signals and exclude background and non-specific staining.

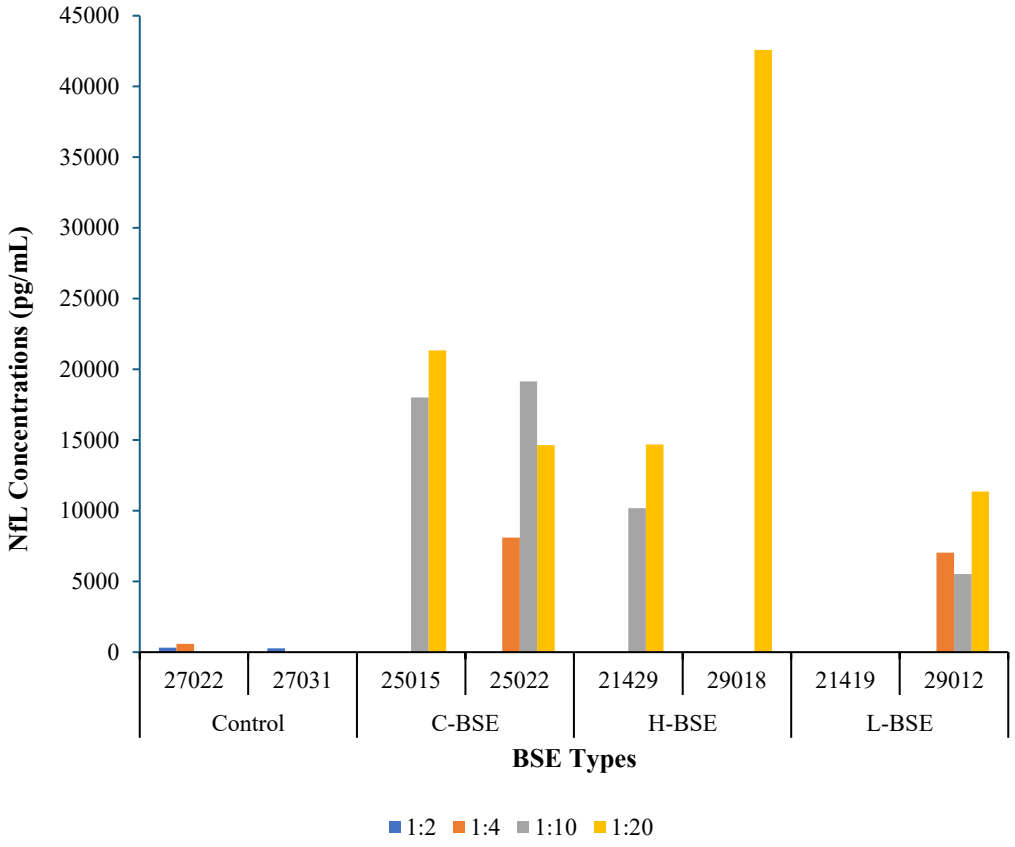

Supplementary Figure 4: Pilot tests to determine optimal dilutions for measuring NfL in cattle CSF using the CSF-NfL human-derived kit. The preliminary test included negative control, C-BSE, H-BSE (n=2 for each), and L-BSE (n=1), using four dilutions: 2-, 4-, 10-, and 20-fold.

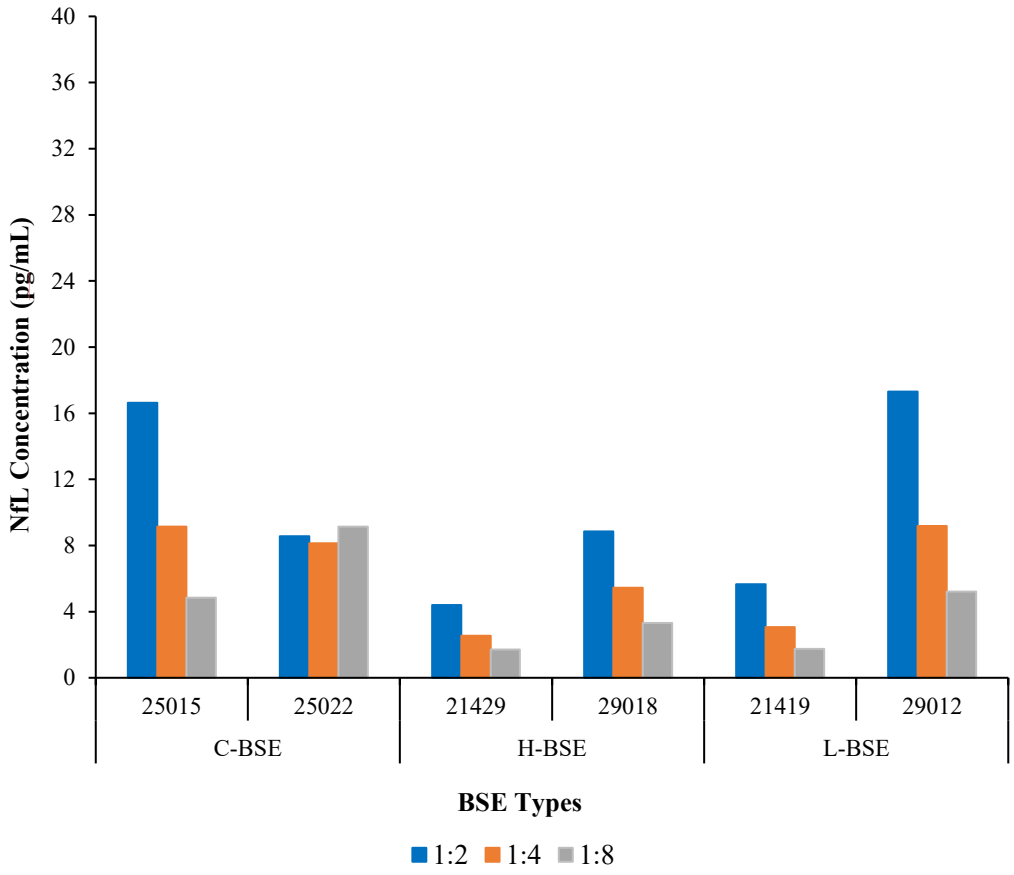

Supplementary Figure 5: Pilot tests to determine optimal dilutions for measuring serum NfL in cattle using a human-derived serum NfL kit. The preliminary test included C-BSE and H-BSE, with n=2 per group, using three dilutions: 2-, 4-, and 8-fold.

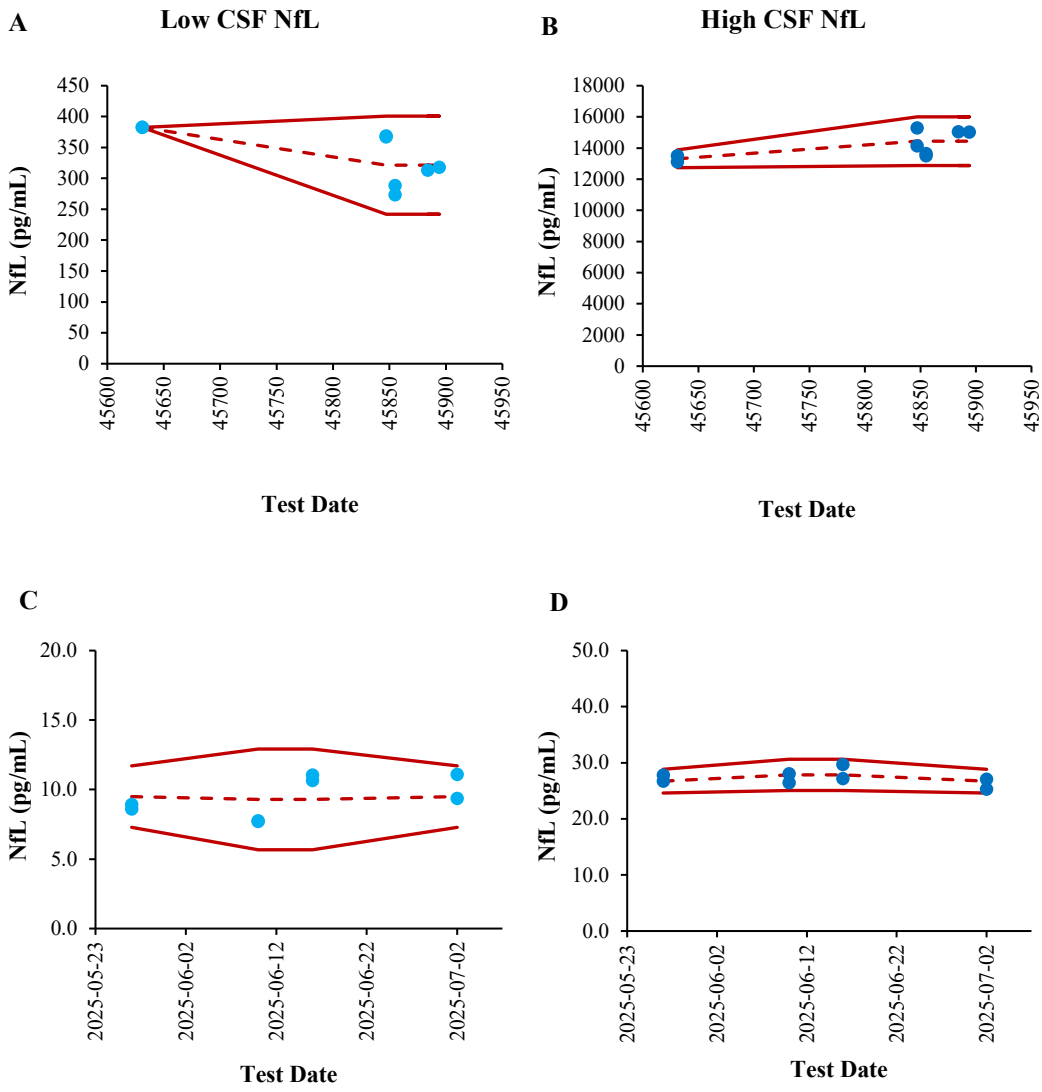

Supplementary Figure 6: Control tracking charts illustrating inter-assay variability of neurofilament light (NfL) concentrations in cerebrospinal fluid (CSF) and serum samples generated using a different kit lots. (A) Low NfL levels in CSF; (B) high NfL levels in CSF; (C) low NfL levels in serum; and (D) high NfL levels in serum.

References:

1. Prusiner, S.B., *Novel proteinaceous infectious particles cause scrapie.* Science, 1982. **216**(4542): p. 136-144.

2. DeArmond, S.J. and S.B. Prusiner, *Etiology and pathogenesis of prion diseases.* The American Journal of Pathology, 1995. **146**(4): p. 785-811.

3. Collinge, J., *Human prion diseases and Bovine Spongiform Encephalopathy (BSE).* Human Molecular Genetics, 1997. **6**(10): p. 1699-705.

4. Williams, E.S.Y., S., *Chronic Wasting Disease of captive mule deer: a Spongiform Encephalopathy.* Journal of Wildlife Diseases, 1980. **16**(1): p. 89-98.

5. Pan, K.M., et al., *Conversion of alpha-helices into beta-sheets features in the formation of the scrapie prion proteins.* Proceedings of the National Academy of Sciences of the United States of America, 1993. **90**(23): p. 10962-10966.

6. Brown, P. and C.R. Abee, *Working with Transmissible Spongiform Encephalopathy agents.* ILAR Journal, 2005. **46**(1): p. 44-52.

7. Prusiner, S.B., *Prions.* Proceedings of the National Academy of Sciences of the United States of America, 1998. **95**(23): p. 13363-13383.

8. Riesner, D., *Biochemistry and structure of PrP(C) and PrP(Sc).* British Medical Bulletin, 2003. **66**: p. 21-33.

9. Kocisko, D.A., et al., *Cell-free formation of protease-resistant prion protein.* Nature, 1994. **370**(6489): p. 471-4.

10. Lawson, V.A., et al., *N-terminal truncation of prion protein affects both formation and conformation of abnormal protease-resistant prion protein generated in vitro.* Journal of Biological Chemistry, 2001. **276**(38): p. 35265-71.

11. Das, A.S. and W.Q. Zou, *Prions: beyond a single protein.* Clinical Microbiology Reviews, 2016. **29**(3): p. 633-58.

12. Sigurdson, C.J., J.C. Bartz, and M. Glatzel, *Cellular and molecular mechanisms of prion disease.* Annual Review of Pathology, 2019. **14**: p. 497-516.

13. McKinnon, C., et al., *Prion-mediated neurodegeneration is associated with early impairment of the ubiquitin-proteasome system.* Acta Neuropathologica, 2016. **131**(3): p. 411-25.

14. Moreno, J.A., et al., *Sustained translational repression by eIF2α-P mediates prion neurodegeneration.* Nature, 2012. **485**(7399): p. 507-11.

15. Xu, Y., et al., *Activation of the macroautophagic system in scrapie-infected experimental animals and human genetic prion diseases.* Autophagy, 2012. **8**(11): p. 1604-20.

16. Resenberger, U.K., et al., *The cellular prion protein mediates neurotoxic signalling of β-sheet-rich conformers independent of prion replication.* The Embo Journal, 2011. **30**(10): p. 2057-70.

17. Laurén, J., et al., *Cellular prion protein mediates impairment of synaptic plasticity by amyloid-beta oligomers.* Nature, 2009. **457**(7233): p. 1128-32.

18. Solforosi, L., et al., *Toward molecular dissection of PrPC-PrPSc interactions.* Journal of Biological Chemistry, 2007. **282**(10): p. 7465-71.

19. Um, J.W., et al., *Alzheimer amyloid-β oligomer bound to postsynaptic prion protein activates Fyn to impair neurons.* Nature Neuroscience, 2012. **15**(9): p. 1227-35.

20. Um, J.W., et al., *Metabotropic glutamate receptor 5 is a coreceptor for Alzheimer aβ oligomer bound to cellular prion protein.* Neuron, 2013. **79**(5): p. 887-902.

21. Kumagai, S., T. Daikai, and T. Onodera, *Bovine Spongiform Encephalopathy – A Review from the Perspective of Food Safety.* Food Safety (Tokyo), 2019. **7**(2): p. 21-47.

22. Haley, N.J. and J.A. Richt, *Classical Bovine Spongiform Encephalopathy and Chronic Wasting Disease: two sides of the prion coin.* Animal Diseases, 2023. **3**(1): p. 24.

23. Wulf, M.-A., A. Senatore, and A. Aguzzi, *The biological function of the cellular prion protein: an update.* BMC Biology, 2017. **15**(1): p. 34.

24. Lee, J., et al., *Prion diseases as transmissible zoonotic diseases.* Osong Public Health and Research Perspectives, 2013. **4**(1): p. 57-66.

25. Moens, A., *Mad cow: a case study in canadian-american relations*. 2006.

26. Amin, R., et al., *Bovine spongiform encephalopathy, "Mad Cow's Disease" and variant creutzfeldt-jakob disease in humans: a critical update.* Archives of medical research, 2023. **54**(5): p. 102854.

27. Kao, R.R., et al., *Epidemiological implications of the susceptibility to BSE of putatively resistant sheep.* The Journal of General Virology, 2003. **84**(Pt 12): p. 3503-3512.

28. Khalil, M., et al., *Neurofilaments as biomarkers in neurological disorders.* Nature Reviews Neurology, 2018. **14**(10): p. 577-589.

29. World Organisation for Animal Health (WOAH), *BSE Risk Categorization*, in *Government of Canada*. 2021.

30. Agency, C.F.I., *Confirmed cases of bovine spongiform encephalopathy (BSE)*. 2025.

31. Hamir, A.N., et al., *Experimental interspecies transmission studies of the Transmissible Spongiform Encephalopathies to cattle: comparison to Bovine Spongiform Encephalopathy in cattle.* Journal of veterinary diagnostic investigation : official publication of the American Association of Veterinary Laboratory Diagnosticians, Inc, 2011. **23**(3): p. 407-20.

32. Government of Saskatchewan, *Bovine Spongiform Encephalopathy (BSE),* 2024.

33. Ricci, A., et al., *Updated quantitative risk assessment (QRA) of the BSE risk posed by processed animal protein (PAP).* EFSA journal. European Food Safety Authority, 2018. **16**(7): p. e05314.

34. Cooley, W.A., et al., *Evaluation of a rapid western immunoblotting procedure for the diagnosis of Bovine Spongiform Encephalopathy (BSE) in the UK.* Journal of Comparative Pathology, 2001. **125**(1): p. 64-70.

35. Olech, M., *Conventional and state-of-the-art detection methods of bovine spongiform encephalopathy (BSE).* International Journal of Molecular Sciences, 2023. **24**(8).

36. Bendheim, P.E., et al., *Nearly ubiquitous tissue distribution of the scrapie agent precursor protein.* Neurology, 1992. **42**(1): p. 149-56.

37. Budka, H., *Neuropathology of prion diseases.* British Medical Bulletin, 2003. **66**(1): p. 121-130.

38. Poggiolini, I., D. Saverioni, and P. Parchi, *Prion protein misfolding, strains, and neurotoxicity: an update from studies on mammalian prions.* International Journal of Cell Biology, 2013. **2013**: p. 910314.

39. Konold, T., et al., *Clinical findings in 78 suspected cases of Bovine Spongiform Encephalopathy in Great Britain.* The Veterinary Record, 2004. **155**(21): p. 659-66.

40. Wells, G.A., et al., *A novel progressive Spongiform Encephalopathy in cattle.* The Veterinary record, 1987. **121**(18): p. 419-420.

41. *CHAPTER 3.4.5 Bovine Spongiform Encephalopathy* WOAH Terrestrial Manual, 2021.

42. *World Organization for Animal Health (OIE).* .

43. Biacabe, A.G., et al., *Distinct molecular phenotypes in bovine prion diseases.* EMBO Reports, 2004. **5**(1): p. 110-5.

44. Dudas, S., et al., *Molecular, biochemical and genetic characteristics of BSE in Canada.* PLoS One, 2010. **5**(5): p. e10638.

45. Schmitz, M., et al., *Validation of plasma and CSF neurofilament light chain as an early marker for sporadic Creutzfeldt-Jakob Disease.* Molecular Neurobiology, 2022. **59**(9): p. 1-9.

46. Steinacker, P., et al., *Neurofilaments in blood and CSF for diagnosis and prediction of onset in Creutzfeldt-Jakob Disease.* Scientific Reports, 2016. **6**: p. 38737.

47. Brown, Q., et al., *Temporal serum neurofilament light chain concentrations in sheep inoculated with the agent of classical Scrapie.* PLoS One, 2024. **19**(2): p. e0299038.

48. Yuan, A., et al., *Neurofilaments and neurofilament proteins in health and disease.* Cold Spring Harbor Perspectives in Biology, 2017. **9**(4).

49. Budelier, M.M., et al., *A map of neurofilament light chain species in brain and cerebrospinal fluid and alterations in Alzheimer's disease.* Brain Communications, 2022. **4**(2): p. fcac045.

50. Petzold, A., *Neurofilament phosphoforms: surrogate markers for axonal injury, degeneration and loss.* Journal of the Neurological Science, 2005. **233**(1-2): p. 183-98.

51. Olney, N.T., S. Spina, and B.L. Miller, *Frontotemporal dementia.* Neurologic Clinics, 2017. **35**(2): p. 339-374.

52. van der Ende, E.L., et al., *Serum neurofilament light chain in genetic frontotemporal dementia: a longitudinal, multicentre cohort study.* The Lancet Neurology, 2019. **18**(12): p. 1103-1111.

53. Carmona-Iragui, M., et al., *Diagnostic and prognostic performance and longitudinal changes in plasma neurofilament light chain concentrations in adults with Down syndrome: a cohort study.* The Lancet Neurology, 2021. **20**(8): p. 605-614.

54. McCombe, P.A., et al., *Serial measurements of phosphorylated neurofilament-heavy in the serum of subjects with amyotrophic lateral sclerosis.* Journal of the Neurological Sciences, 2015. **353**(1): p. 122-129.

55. Fast, C., et al., *Discrimination of classical and atypical BSE by a distinct immunohistochemical PrP(Sc) profile.* Pathogens, 2023. **12**(2).

56. Meloni, D., et al., *EU-approved rapid tests for bovine spongiform encephalopathy detect atypical forms: a study for their sensitivities.* PLoS One, 2012. **7**(9): p. e43133.

57. Shaw, G., et al., *Uman-type neurofilament light antibodies are effective reagents for the imaging of neurodegeneration.* Brain Communication, 2023. **5**(2): p. fcad067.

58. Betancor, M., et al., *Neurogranin and Neurofilament light chain as preclinical biomarkers in scrapie.* International Journal of Molecular Science, 2022. **23**(13).

59. Zetterberg, H., et al., *Neurofilaments in blood is a new promising preclinical biomarker for the screening of natural scrapie in sheep.* PLoS One, 2019. **14**(12): p. e0226697.

60. Thompson, A.G.B., et al., *Neurofilament light chain and tau concentrations are markedly increased in the serum of patients with sporadic Creutzfeldt-Jakob disease, and tau correlates with rate of disease progression.* Journal of Neurology, Neurosurgery, and Psychiatry, 2018. **89**(9): p. 955-961.

61. Whitlock, M.C.S., Dolph, *The analysis of biological data, the normal distribution.* 2020: p. 231-255.

62. Whitlock, M.C.S., Dolph, *The analysis of biological data.* 2020: p. 301.

63. Khalil, M., et al., *Serum neurofilament light levels in normal aging and their association with morphologic brain changes.* Nature Communications, 2020. **11**(1): p. 812.

64. Kübler, E., B. Oesch, and A.J. Raeber, *Diagnosis of prion diseases.* British Medical Bulletin, 2003. **66**: p. 267-79.

65. Ferrer, I., *Biological fluid biomarkers in human prion diseases with a note on biosafety.* Subcellular Biochemistry, 2025. **112**: p. 189-217.

66. Koníčková, D., et al., *RT-QuIC: a highly promising diagnostic method for neurodegenerative diseases-advantages and limitations.* Frontiers in Neurology, 2025. **16**: p. 1578252.

67. Lattanzio, F., et al., *Prion-specific and surrogate CSF biomarkers in Creutzfeldt-Jakob disease: diagnostic accuracy in relation to molecular subtypes and analysis of neuropathological correlates of p-tau and Aβ42 levels.* Acta Neuropathologica, 2017. **133**(4): p. 559-578.

68. Atarashi, R., et al., *Ultrasensitive human prion detection in cerebrospinal fluid by real-time quaking-induced conversion.* Nat Med, 2011. **17**(2): p. 175-8.

69. Figgie, M.P., Jr. and B.S. Appleby, *Clinical use of improved diagnostic testing for detection of prion disease.* Viruses, 2021. **13**(5).

70. Eraña, H., et al., *Detection of pathognomonic biomarker PrP(Sc) and the contribution of cell free-amplification techniques to the diagnosis of prion diseases.* Biomolecules, 2020. **10**(3).

71. Abu-Rumeileh, S., et al., *Diagnostic value of surrogate CSF biomarkers for Creutzfeldt-Jakob disease in the era of RT-QuIC.* Journal of Neurology, 2019. **266**(12): p. 3136-3143.

72. Gmitterová, K., et al., *Cerebrospinal fluid markers in the differentiation of molecular subtypes of sporadic Creutzfeldt-Jakob disease.* Eur J Neurol, 2016. **23**(6): p. 1126-33.

73. Blennow, K., et al., *Tau protein in cerebrospinal fluid: a biochemical marker for axonal degeneration in Alzheimer disease?* Molecular and Chemical Neuropathology, 1995. **26**(3): p. 231-45.

74. Morenas-Rodríguez, E., et al., *Soluble TREM2 in CSF and its association with other biomarkers and cognition in autosomal-dominant Alzheimer's disease: a longitudinal observational study.* The Lancet Neurology, 2022. **21**(4): p. 329-341.

75. Minikel, E.V., et al., *Domain-specific quantification of prion protein in cerebrospinal fluid by targeted mass spectrometry.* Molecular and Cellular Proteomics: MCP, 2019. **18**(12): p. 2388-2400.

76. Barba, L., et al., *CSF synaptic biomarkers in AT(N)-based subgroups of lewy body disease.* Neurology, 2023. **101**(1): p. e50-e62.

77. Muñoz-García, M.I., et al., *Synaptic dysfunction and glial activation markers throughout aging and early neurodegeneration: a longitudinal CSF biomarker-based study.* Molecular Neurodegeneration, 2025. **20**(1): p. 109.

78. Bargar, C., et al., *Streamlined alpha-synuclein RT-QuIC assay for various biospecimens in Parkinson's disease and dementia with lewy bodies.* Acta Neuropathologica Communication, 2021. **9**(1): p. 62.

79. Abu-Rumeileh, S., et al., *CSF Beta-Synuclein, SNAP-25, and Neurogranin in Infectious and Autoimmune Inflammatory Neurologic Diseases.* Neurology (R) Neuroimmunology & Neuroinflammation, 2025. **12**(6): p. e200491.

80. Mastrangelo, A., et al., *Diagnostic and prognostic performance of CSF α-synuclein in prion disease in the context of rapidly progressive dementia.* Alzheimers Dement (Amst), 2021. **13**(1): p. e12214.

81. Obst, J., et al., *The role of microglia in prion diseases: A paradigm of functional diversity.* Frontiers in Aging Neuroscience, 2017. **9**: p. 207.

82. Fujita, K., et al., *Increased interleukin-17 in the cerebrospinal fluid in sporadic Creutzfeldt-Jakob disease: a case-control study of rapidly progressive dementia.* Journal of Neuroinflammation, 2013. **10**: p. 135.

83. Denk, J., et al., *MicroRNA profiling of CSF reveals potential biomarkers to detect Alzheimer`s disease.* PLoS One, 2015. **10**(5): p. e0126423.

84. López-Pérez, Ó., et al., *Cerebrospinal fluid and plasma small extracellular vesicles and miRNAs as biomarkers for prion diseases.* International Journal of Molecular Sciences, 2021. **22**(13).

85. Thompson, A.G.B., et al., *Evaluation of plasma tau and neurofilament light chain biomarkers in a 12-year clinical cohort of human prion diseases.* Molecular Psychiatry, 2021. **26**(10): p. 5955-5966.

86. Zerr, I., et al., *Diagnostic and prognostic value of plasma neurofilament light and total-tau in sporadic Creutzfeldt-Jakob Disease.* Alzheimers Research & Therapy, 2021. **13**(1): p. 86.

87. Giacomucci, G., et al., *Plasma neurofilament light chain as a biomarker of Alzheimer's disease in Subjective Cognitive Decline and Mild Cognitive Impairment.* Journal of Neurology, 2022. **269**(8): p. 4270-4280.

88. Forgrave, L.M., et al., *The diagnostic performance of neurofilament light chain in CSF and blood for Alzheimer's disease, frontotemporal dementia, and amyotrophic lateral sclerosis: A systematic review and meta-analysis.* Alzheimer's & Dementia: Diagnosis, Assessment & Disease Monitoring, 2019. **11**: p. 730-743.

89. Liu, Y., et al., *Neurofilament light as a biomarker for motor decline in Parkinson's disease.* Frontiers in Neuroscience, 2022. **16**: p. 959261.

90. Shahim, P., et al., *Neurofilament light as a biomarker in traumatic brain injury.* Neurology, 2020. **95**(6): p. e610-e622.

91. Alagaratnam, J., et al., *Correlation between CSF and blood neurofilament light chain protein: a systematic review and meta-analysis.* BMJ Neurology Open, 2021. **3**(1): p. e000143.

92. Abu-Rumeileh, S. and P. Parchi, *Cerebrospinal fluid and blood Neurofilament light chain protein in prion disease and other rapidly progressive dementias: current state of the art.* Frontiers in Neuroscience, 2021. **15**: p. 648743.

93. Priemer, G., et al., *Biochemical characteristics and PrP(Sc) distribution pattern in the brains of cattle experimentally challenged with H-type and L-type atypical BSE.* PLoS One, 2013. **8**(6): p. e67599.

94. Adiutori, R., et al., *The proteome of neurofilament-containing protein aggregates in blood.* Biochemistry and Biophys Reports, 2018. **14**: p. 168-177.

95. Brureau, A., et al., *NF-L in cerebrospinal fluid and serum is a biomarker of neuronal damage in an inducible mouse model of neurodegeneration.* Neurobiology of Dissease, 2017. **104**: p. 73-84.

96. Lombardi, V., et al., *The potential of neurofilaments analysis using dry-blood and plasma spots.* Scientific Reports, 2020. **10**(1): p. 97.

97. Devarakonda, S.S., et al., *Molecular mechanisms of neurofilament alterations and its application in assessing neurodegenerative disorders.* Ageing Research Reviews, 2024. **102**: p. 102566.

98. Frigerio, I., et al., *Neurofilament light chain is increased in the parahippocampal cortex and associates with pathological hallmarks in Parkinson's disease dementia.* Transl Neurodegener, 2023. **12**(1): p. 3.

99. Brummer, T., et al., *Spatial transcriptomics and neurofilament light chain reveal changes in lesion patterns in murine autoimmune neuroinflammation.* Journal of Neuroinflammation, 2023. **20**(1): p. 262.

100. Machacek, M., et al., *NfL concentration in CSF is a quantitative marker of the rate of neurodegeneration in aging and Huntington's disease: a semi-mechanistic model-based analysis.* Frontiers in Neuroscience, 2024. **18**: p. 1420198.

101. Kahn, O.I., et al., *Secreted neurofilament light chain after neuronal damage induces myeloid cell activation and neuroinflammation.* Cell Reports, 2025. **44**(3): p. 115382.

102. Nixon, R.A., *Autophagy in neurodegenerative disease: friend, foe or turncoat?* Trends in Neuroscience, 2006. **29**(9): p. 528-35.

103. Wang, Q.J., et al., *Induction of autophagy in axonal dystrophy and degeneration.* Journal of Neuroscience: , 2006. **26**(31): p. 8057-68.

104. Bridel, C., et al., *Diagnostic value of cerebrospinal fluid Neurofilament light protein in neurology: a systematic review and meta-analysis.* JAMA Neurology, 2019. **76**(9): p. 1035-1048.

105. Gaetani, L., et al., *Neurofilament light chain as a biomarker in neurological disorders.* Journal of Neurology, Neurosurgery, and Psychiatry, 2019. **90**(8): p. 870-881.

106. Hagberg, L., H. Zetterberg, and M. Gisslén, *Neurofilament light chain as a biomarker for neuronal injury in CNS infections.* Expert Review of Molecular Diagnostics, 2025. **25**(8): p. 419-424.

107. van Zeggeren, I.E., et al., *Neurofilament light chain in central nervous system infections: a prospective study of diagnostic accuracy.* Scientific Reports, 2022. **12**(1): p. 14140.

108. Badiola, J.J., *Bovine spongiform encephalopathy.* PROFESSIONAL VERSION, 2024.